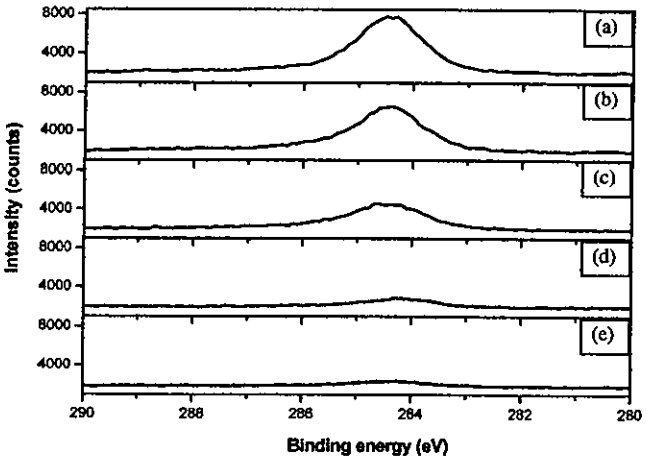


**Figure 5.** XPS C 1s peaks: (a) unirradiated ODS SAM, (b) after 45 s of irradiation, (c) after 90 s of irradiation, (d) after 120 s of irradiation, and (e) the clean $SiO_2$/Si substrate.

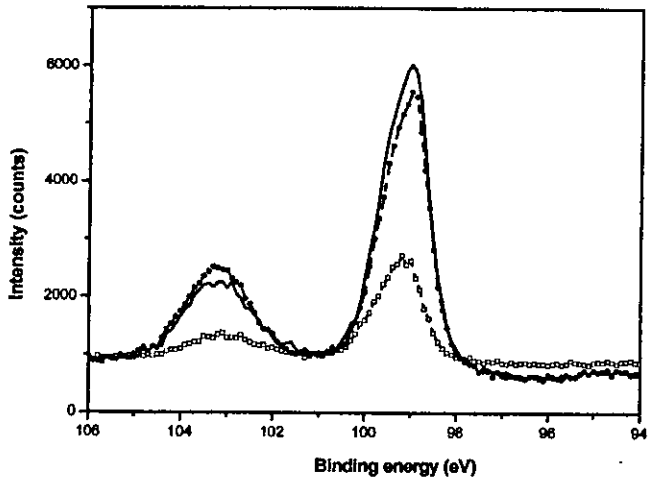


**Figure 6.** XPS Si 2p region. The solid lines with open squares show the unirradiated ODS SAM, the solid lines with circles show the irradiated ODS SAM after 120 s of irradiation time, and the continuous curve shows the photocleaned substrate.

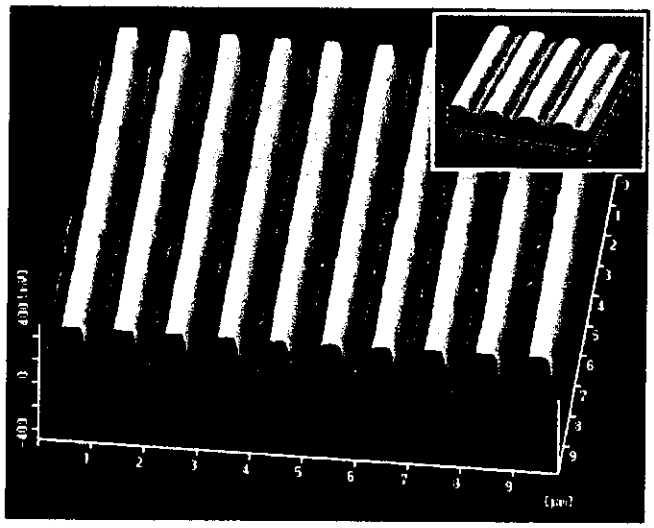

**Figure 7.** Lateral force microscopy image of the line-space patterned region.

irradiation for 120 s, indicating that photoirradiated surfaces became completely hydrophilic.

**XPS Results.** We also confirmed based on XPS measurements that the carbon intensity level on the photoirradiated SAM surfaces decreased with photoirradiation time. Figure 4 presents the carbon/silicon (C/Si) intensity ratio as a function of irradiation time. The ratio decreases with irradiation time. The decrease in the C/Si ratio can be attributed to a reduction in the amount of carbon within the converted surface film.

Figure 5 shows C 1s XPS narrow scans of the unirradiated and irradiated ODS SAMs as well as a spectrum of a photochemically cleaned Si surface. The peak in the C 1s spectrum of the undegraded ODS SAM was assigned to emissions from alkyl chains. After laser irradiation, the peak intensity of the alkyl chains has decreased since ODS molecules were removed gradually. The intensity after 120 s of irradiation (spectrum d) becomes almost equal to that of a clean Si surface, prior to SAM deposition, i.e., a background level (spectrum e). The origin of C 1s signals from the cleaned Si surface is carbon contamination adsorbed prior to the XPS measurement. Such contamination most likely had to be adsorbed on the irradiated SAM surface as well. Oxidized products, such as −COOH and −CHO groups, do not appear at 287−289 eV in the C 1s XPS spectra.[27] Although further detailed research is needed, lithography at 157 nm looks promising for patterning a large variety of SAMs, since it may depend on photoinduced cleavage of C−C bonds and subsequent decomposition of organic molecules.[14] Figure 6 shows the narrow scan of the Si 2p region. The solid lines with open squares show the unirradiated ODS SAM, the solid lines with circles show the irradiated ODS SAM after 120 s of irradiation time, and the continuous curve shows the photocleaned substrate. With increasing irradiation time, the intensities of both the Si peak at 99.3 eV and the Si−O peak at 103.3 eV increase, approaching the values for the clean substrate.

**SPM Results.** Figure 7 shows a 10 $\mu$m × 10 $\mu$m LFM image consisting of lines and spaces having a width of 500 nm each. Such a clear pattern was observed on larger surfaces too (not shown here), up to the maximum range of 150 $\mu$m × 150 $\mu$m of the SPM scan head and within the total patterned area of around 3 mm × 3 mm dictated by the aperture of the laser. A larger value for the friction force is representative for photodegraded areas.[28] These areas, which exhibited stronger lateral force than the hydrophobic, undegraded SAM surfaces, had to be hydrophilic as shown in Figure 4. Hydrophilic regions of photodegraded SAMs chemically interact with the AFM-probe surface, which due to its surface oxide is also hydrophilic, leading to higher friction values. In such a case, hydrogen bondings may form between the sample and probe surfaces.

An inevitable shortcoming of photolithography is that its patterning resolution is degraded by penumbral blurring effects together with diffraction and reflection of light. The inset in Figure 7 shows, for clarity, a 4 $\mu$m × 4 $\mu$m area. At the top of the unirradiated regions, an additional thin line is visible. We believe this line to be caused by laser light diffraction at the edge of the chromium pattern on the photomask. Despite this undesirable effect, the width of this line is estimated to be around 100 nm, providing an indication that the photolithographic process can create 100 nm features, or even less, on ODS SAMs.

Topographies of the patterned SAMs were also acquired in order to provide more insight into the process that took

(27) Beamson, G.; Briggs, D. *High-Resolution XPS of Organic Polymers*; John Wiley & Sons: Chichester, 1992.

(28) Sugimura, H.; Nakagiri, N. *Appl. Phys. A* **1998**, *66*, S427.

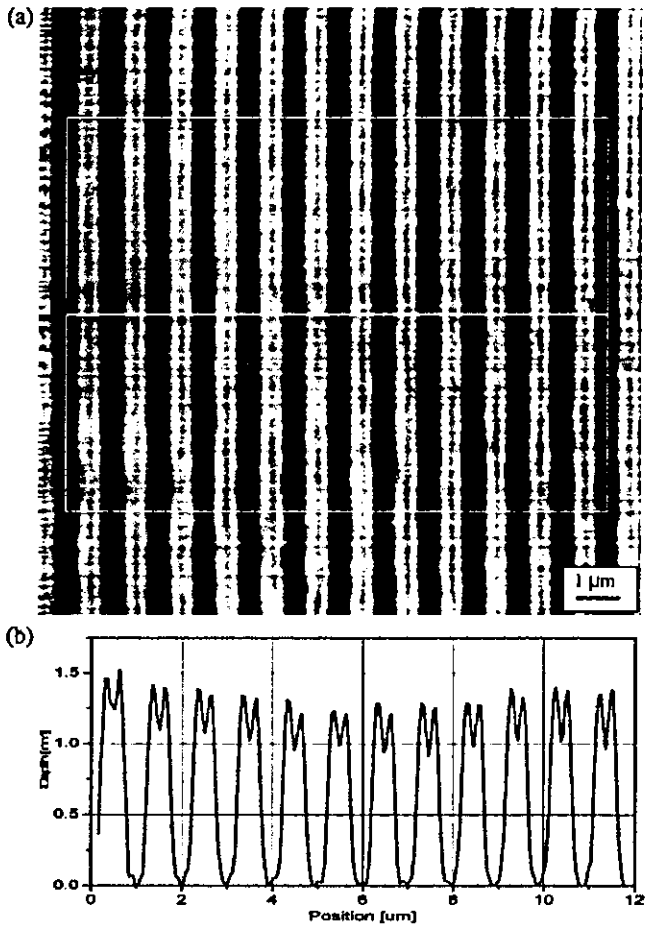


**Figure 8.** (a) Atomic force microscopy image corresponding to the region in Figure 7; (b) average cross-section profile for the area delimited by the thin white line in panel a.

place in the photoirradiated areas. As seen in Figure 8, photoirradiated regions are recessed from the surrounding unirradiated regions. Recessed depths determined from cross sections of the AFM images were $1.4 \pm 0.1$ nm. These depths were smaller than ellipsometry-measured SAMs thicknesses, i.e., 1.68–1.7 nm. That is because a thin layer of $SiO_x$ remains on the substrate even when all organic parts are removed.[29] The thickness of the remaining $SiO_x$ layer was estimated by ellipsometry to be ca. 0.2 nm. Therefore, ODS SAMs were concluded to be photodecomposed and removed in the photoirradiated regions.

## Conclusions

Using a molecular fluorine laser at 157 nm wavelength, submicron patterning of organosilane SAMs was successfully demonstrated on the basis of photolithography. An organosilane, namely, ODS, was chosen to create by chemisorption a SAM onto an oxide-covered Si substrate, which SAM was subsequently patterned using the laser. After an initial air evacuation, the optical path of the laser beam and the photomask–sample space were backfilled and then purged with nitrogen. The photoirradiation process and the resulting pattern were investigated using XPS, SPM, ellipsometry, and contact angle measurements. The acquired SPM images show that 500 nm size features can be successfully photoprinted in this way.

Potential applications can be identified in the field of electronic devices, organic templates, and so forth. These promising initial results will be further investigated to check the validity of the approach, to quantify the necessary laser fluence for optimal photoirradiation of the SAM, and to identify possible bottlenecks such as, for instance, contamination problems resulting from the long-term exposure of the optical path to various organic compounds.

**Acknowledgment.** This study was partially supported by the Aichi Science and Technology Foundation.

LA0480944

(29) Brunner, H.; Vallant, T.; Mayer, U.; Hoffmann, H. *Langmuir* **1996**, *12*, 4614–4617.

# Generation of Amino-Terminated Surfaces by Chemical Lithography Using Atomic Force Microscopy

N. Saito,*,† N. Maeda,† H. Sugimura,† and O. Takai‡

*Department of Materials Engineering, Graduate School of Engineering, Nagoya University, Furo-cho, Chikusa-ku, Nagoya 464-8603, Japan, and Center for Integrated Research in Science and Engineering, Nagoya University, Furo-cho, Chikusa, Nagoya 464-8603, Japan*

*Received July 23, 2003. In Final Form: January 30, 2004*

Self-assembled monolayers (SAMs) covered with nitroso end groups were reduced using an atomic force microscope. As the bias voltage become more negative (beyond −4 V), the surface potential of the scanned area become closer to that of the amino-terminated SAM. Following this chemical change, however, no change in topographic features was detected, implying retained stability of the underlying SAM layer. We then released carboxylate-modified polystyrene (PS) spheres into a pH 4 solution containing the sample. Subsequent imaging with atomic force microscopy (AFM) revealed that these PS spheres were only selectively immobilized on the regions that were originally scanned at −6 V to form amino termination. In summary, using AFM set to a specific voltage, we were able to selectively generate micropatterned regions of the SAM with amino termination.

## Introduction

Amino-terminated self-assembled monolayers (SAMs) on silicon substrate have a potential as templates for biosensor or molecular devices. Since amino groups are able to link with target molecules such as deoxyribonucleic acid (DNA) and antibody-forming cell, many researchers had investigated amino-terminated SAMs.[1−5] To fabricate components of future microdevices, such templates might offer high chemical reactivity which is restricted to specific microregions. Thus, the amino-terminated regions must be prepared on given points of a substrate.

Such a microstructure can be accomplished by maskless lithography techniques such as focus ion beam and electron beam lithography techniques.[6−10] However, these lithography techniques cause radiation damage to the amino-terminated surface of a SAM due to the excessive energy applied. To overcome these problems, we developed a soft chemical lithography process for the generation of amino-terminated surface, that is, a technique which would convert only the functional groups. Scanning probe lithography (SPL) is based on an electrochemical approach and can be employed to realize such a soft process by controlling the applied potential.[11,12] SPL had been applied in many cases, however, for the elimination of SAMs.

In our present research, we have attempted through chemical lithography to use an atomic force microscope to produce amino-terminated regions on a sample surface without damage to the molecule. To realize this, we focused out attention on the reactivity of the amino-terminated surface, as described below. The amino-terminated surface is first oxidized by heating in air. Following this, a positive potential is electrochemically applied beyond the oxidation−reduction (OR) potential. The nitroso- or nitro-terminated surface can be converted back into an amino-terminated surface by applying electrochemical negative potential below the OR potential.

In this investigation, an amino-terminated SAM was prepared from (*p*-aminophenyl)trimethoxysilane (APhS) though chemical vapor deposition (CVD). The root mean square (rms) of APhS-SAM was 0.32 nm, which was approximately equal to the rms of silicon wafer. This was then first oxidized by heating in air. Next, the oxidized surface was then converted into an amino-terminated surface by chemical lithography. The functional groups on the surfaces thus obtained by chemical lithography were confirmed by selectively labeling the carboxyl-terminated latex particles in order to detect the amino groups.

## Experimental Section

The APhS-SAMs were prepared on the substrates of n-type silicon by CVD.[13] A silicon surface covered with a thin oxide layer (ca. 2 nm) was hydroxylated and cleaned simultaneously by a UV/ozone cleaning method. The substrates were then heated together with a container of APhS in an oven, thus depositing APhS-SAMs when the precursor reacted with the hydroxyls on the substrate surfaces. The reaction temperature was 373 K, and the reaction time was 1 h.

Chemical lithography was conducted with an atomic force microscope (Seiko Instruments Inc., SPA-300HV + SPI-3800N) in air. The force constant of gold-coated silicon cantilever was

† Department of Materials Engineering, Graduate School of Engineering, Nagoya University.

‡ Center for Integrated Research in Science and Engineering, Nagoya University.

(1) Petri, D. F. S.; Wenz, G.; Schunk, P.; Schimmel, T. *Langmuir* **1997**, *15*, 4520−4523.

(2) Yang, Z.; Frey, W.; Oliver, T.; Chilkoti, A. *Langmuir* **2000**, *16*, 1751−1758.

(3) Turyan, I.; Matsue, T.; Mandler, D. *Anal. Chem.* **2000**, *72*, 3431−3435.

(4) Geyer, W.; Stadler, V.; Eck, W.; Golzhauser, A.; Grunze, M.; Sauer, M.; Weimann, T.; Hinze, P. *J. Vac. Sci. Technol., B* **2001**, *19*, 2732−2735.

(5) Chirakul, P.; Perez-Luna, V. H.; Owen, H.; Lopez, G. P. *Langmuir* **2002**, *18*, 4234−4330.

(6) Pan, M.; Yun, M.; Kozicki, M. N.; Whidden, T. K. *Superlattices Microstruct.* **1996**, *20*, 369−376.

(7) Ada, E. T.; Hanley, L.; Etchin, S.; Melngailis, J.; Dressick, W. J.; Chen, M. S.; J. M. Calvert, J. M. *J. Vac. Sci. Technol., B* **1995**, *13*, 2189−2196.

(8) Lercel, M. J.; Whelan, C. S.; Craighead, H. G.; Seshadri, K.; Allara, D. L. *J. Vac. Sci. Technol., B* **1996**, *14*, 4085−4090.

(9) Kidoaki, S.; Matsuda, T. *Langmuir* **1999**, *15*, 7639−7646.

(10) Harnett, C. K.; Satyalakshmi, K. M.; Craighead, H. G. *Langmuir* **2001**, *17*, 178−182.

(11) Sugimura, H.; Okiguchi, K.; Nakagiri, N. *Jpn. J. Appl. Phys. 1* **1996**, *35*, 3749−3753.

(12) Xia, Y.; Rogers, J. A.; Paul, K. E.; Whitesides, G. M. *Chem. Rev.* **1999**, *99*, 1823−1848.

(13) Sugimura, H.; Hozumi, A.; Kameyama, T.; Takai, O. *Surf. Interface Anal.* **2002**, *34*, 550−554.

10.1021/la0353428 CCC: $27.50 
Published on Web 05/20/2004

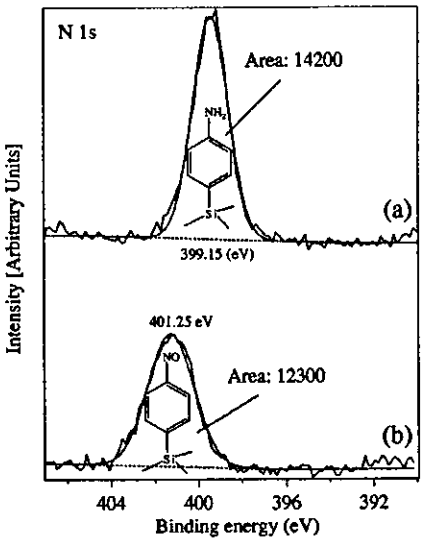


**Figure 1.** XPS N 1s spectra of APhS-SAM: (a) before and (b) after heat treatment.

0.1 N/m (Seiko Instruments Inc., Micro Cantilever, type SI-AF01-A). Bias voltages of −1 to −6 V were applied (the substrate corresponds to a cathode). The SPL areas are a square 20 $\mu$m on a side. After chemical lithography, the sample surfaces were observed in a nitrogen atmosphere with a Kelvin force probe microscope (KPFM) (Seiko Instruments Inc., SPA-300HV+SPI-3800N) using a gold-coated silicon cantilever (Seiko Instruments Inc., Micro Cantilever, type SI-DF3-A). The details of the KPFM measurements were determined on the basis of our previous research.[14] We observed the SPL areas of 20 $\mu$m in KPFM and AFM images (150 $\mu$m × 150 $\mu$m).

Some samples were immersed in a solution dispersed with carboxylate-modified polystyrene fluorescence spheres (CM-FluoSpheres; Molecular Probes, Inc., model F-8888, 0.06% solution in water) for 1 h under mild agitation. After immersion, the samples were rinsed with Mill-Q water and blown dry by $N_2$ gas stream. Dark-field images of the sample surfaces after immobilization were obtained using an optical microscope (Nikon, ECLIPSE-ME600).

## Results and Discussion

The water contact angle of the APhS-SAM became saturated at approximately 60° at the reaction time of 1 h. This value agrees with that obtained in previous reports.[15] Furthermore, the film thickness of 0.6 nm, as determined by ellipsometry, corresponded approximately to the distance from Si to N atoms in the precursor. Figure 1a shows a XPS N 1s spectrum of APhS-SAM. Its peak of 399.1 eV is assigned to the amino group attached to an aromatic ring, as indicated. To clearly demonstrate the presence of the amino group, the APhS-SAM was micropatterned by vacuum ultraviolet lithography, thus dividing the small surface into distinct APhS-SAM and $SiO_x$ regions. The functional groups of the SAM were confirmed by the selective adsorption of carboxylate-modified polystyrene fluorescence spheres in a pH 4 solution.[15] The $-NH_2$ and $-COOH$ groups in the pH 4 solution were converted into $-NH_3^+$ and $-COO^-$ ion groups, so that the selective adsorption of polystyrene spheres on to the substrate proceeded due to their attractive interaction

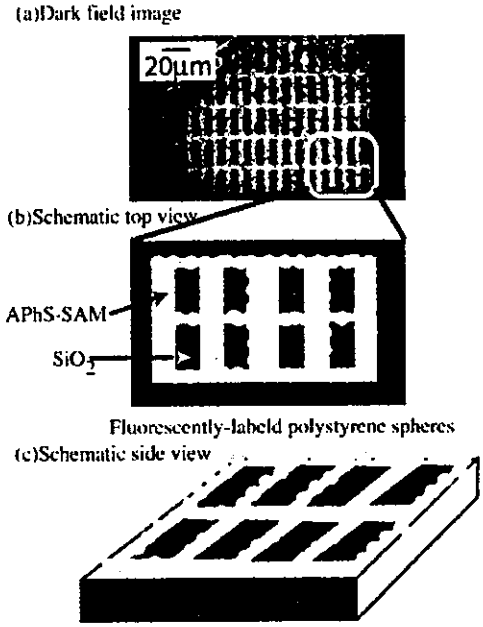


**Figure 2.** Dark field image of micropatterned APhS-SAM/$SiO_2$ sample after immersion in a pH 4 solution containing carboxylate-modified polystyrene fluorescence spheres. Top and bottom views indicating the APhS-SAM and $SiO_2$ regions are also illustrated.

to the surface. Under this pH condition, the regions of silica on the surface were negatively charged and the carboxylate-modified polystyrene fluorescence spheres did not adsorb onto it. Figure 2 shows an image acquired by dark field microscopy of the micropatterned APhS/$SiO_2$ sample after immersion. The lighter areas between the dark rectangular regions correspond to APhS-SAM. This dark-field image indicates that carboxylate-modified polystyrene fluorescence spheres selectively adsorbed on the APhS-SAM since scattered light due to surface roughness can be observed. From these results, we determined that an APhS-SAM had been successfully prepared.

APhS-SAM samples were heated at 350 °C for 3 h in air in order to convert their amino groups into nitroso groups. Figure 1b shows XPS N 1s spectrum of the sample after the heat treatment. The peak areas of the spectra before and after the heat treatment did not greatly change. The center of peak in the spectrum seen in Figure 1b was located at ca. 401 eV, which is assigned to nitroso groups (−NO). Furthermore, we can confirm that the C 1s spectrum after heat treatment was also identical with the spectrum of APhS-SAM. These results indicate that only amino groups were converted into nitroso groups without decomposition of the aromatic rings and siloxane networks.

A gold-coated probe was scanned on nitroso-terminated SAM in air at bias voltages of −1 to −6 V. Parts a−c of Figure 3 show topographic images, surface potential images, and the surface potential profile, respectively. As seen in Figure 3a, no topographic features were detected in this bias range. On the other hand, the surface potential of the probe-scanned area against the nitroso-terminated surface became more positive as the bias voltages became more negative. In particular, the surface potentials changed drastically at ca. −4 V. The amino- and nitroso-terminated surfaces have positive and negative charges, respectively, based on permanent dipole moments. Consequently, the surface potential of the amino-terminated

(14) Hayashi, K.; Saito, N.; Sugimura, H.; Takai, O.; Nakagiri, N. *Langmuir* **2002**, *18*, 7469−7472.
(15) Hayashi, K.; Sugimura, H.; Takai, O. *Appl. Surf. Sci.* **2002**, *188*, 513−518.
(16) Hozumi, A.; Yokogawa, Y.; Kameyama, T.; Sugimura, H.; Hayashi, K.; Shirayama, H.; Takai, O., *J. Vac. Sci. Technol., B* **2001**, *19*, 1812−1816.

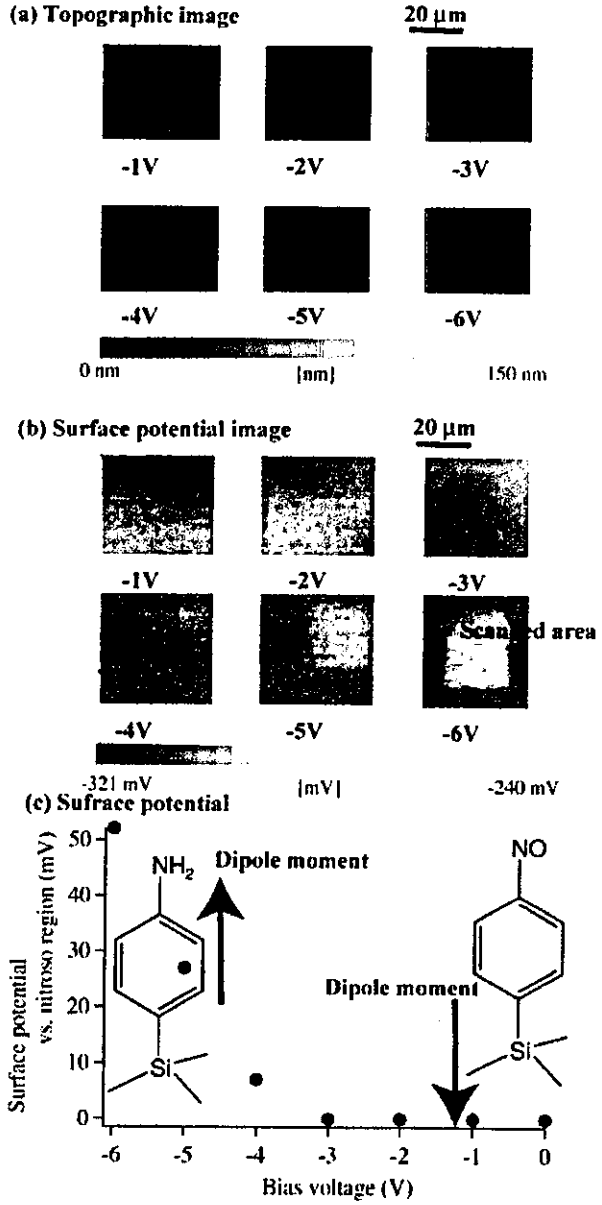


**Figure 3.** Topographic images (a), surface potential images (b), and surface potential profile (c) of nitroso-terminated SAMs chemically modified using AFM, at different bias voltages.

surface is more positive than that of the nitroso-terminated surface. Interpretation of the images in Figure 3 could be as follows. The change in tip potential has direct correlation with the generation of amino groups in the areas scanned where amino groups were generated. To confirm this, we show that carboxylate-modified polystyrene fluorescence spheres immobilize (in a solution of pH 4) on the SPM scanned areas of the sample. The results are shown in the dark field images of Figure 4. Figure 4 shows

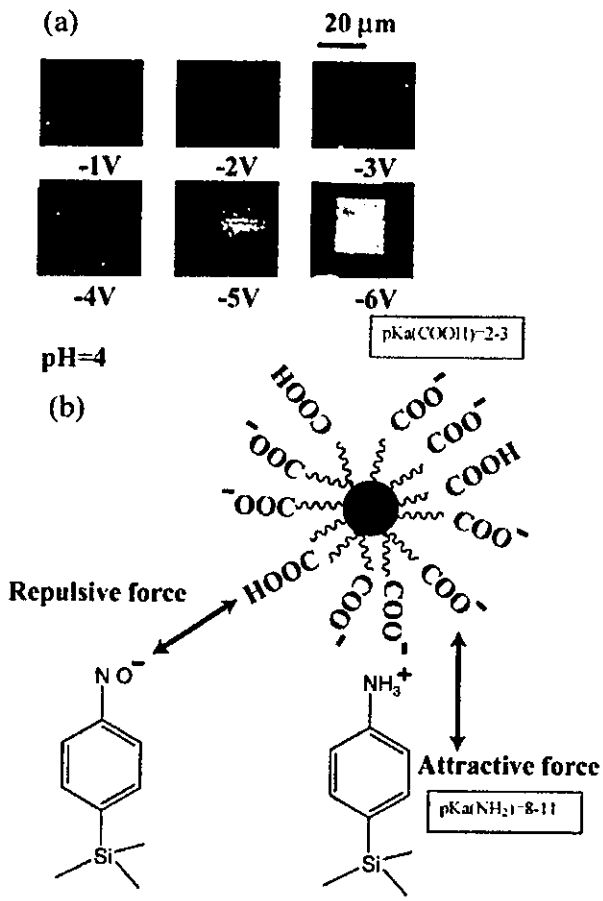


**Figure 4.** Dark field images of chemically lithographed nitroso-terminated SAMs after immersion in a pH 4 solution containing carboxylate-modified, fluorescently labeled polystyrene spheres.

dark field microscopic images of these samples. The fluorescently labeled polystyrene spheres appear to selectively adsorb in areas that were scanned with a bias of −6. These topographic images correlate well with the surface-potential images of Figure 3b. These results demonstrate that our chemical lithography technique selectively generates the amino groups at desired locations at the micrometer-scale on the sample.

In summary, amino-terminated micrometer-scale regions on silicon substrates surfaces were successfully generated by chemical lithography using atomic force microscopy. This technique may prove useful to fabricate biochips on silicon substrates via a bottom up approach, as demonstrated here.

**Acknowledgment.** This work has been supported by the "Biomimetic Materials Processing" (No. JSPS-RFTF 99R13101), Research for the Future (RFTF) Program, Japan Society for the Promotion of Science.

LA0353428

# Chemoenzymatically Synthesized Glycoconjugate Polymers†

Yoshiko Miura,* Takayasu Ikeda, and Kazukiyo Kobayashi

*Department of Molecular Design and Engineering, Graduate School of Engineering, Nagoya University, Furo-cho, Chikusa-ku, Nagoya, Aichi 464-8603, Japan*

*Received October 29, 2002; Revised Manuscript Received January 5, 2003*

Glycoconjugate polymers with poly(vinyl alcohol) (PVA) backbone were synthesized via a chemoenzymatic method. The sugar alcohols of maltose and lactose were submitted to transesterification in the presence of lipases. The esterification was achieved with high selectivity and yield, and the resulting maltitol and lactitol 6-vinyl sebacates were polymerized by a conventional radical initiator with hydrogen peroxide and ascorbic acid. The glycoconjugate polymers carrying α-glucose and β-galactose as recognition signals showed the biological activity such as lectin recognition abilities and hepatocyte adhension. The biodegradability of these polymers was modest but higher than PVA.

## Introduction

Carbohydrates on cell surfaces serve as significant biological signals and play important roles in numerous intercellular recognition processes.[1] However, the interactions of isolated carbohydrate ligands with carbohydrate-binding proteins (lectins) are low in affinity and broad in specificity.[2] The carbohydrate signals in biological system are often amplified by the multivalency of carbohydrates or the "glyco-cluster effect".[3] Synthetic glyco-clusters are also reported to amplify the carbohydrate signals similarly to the natural carbohydrate ligands.[4−6] In particular, synthetic glycoconjugate polymers substituted with pendant saccharide have attracted a great attention as synthetic glyco-clusters.[7] We have investigated artificial glycoconjugate polymers with hydrophobic main chains and hydrophilic pendant carbohydrates. These polymers are reported to form characteristic cylindrical conformation in water due to the amphiphilic properties.[8] The densely packed glyco-clusters exhibited unique biological recognition abilities such as lectin recognition, hepatocyte culture, and virus adsorption. In the present paper, we have elaborated a facile synthesis of glycoconjugate polymers applying enzymatic catalysis that is of greater advantage in terms of chemoselectivity and efficiency and also from the aspects of green chemistry (Figure 1).

Esterases such as lipases and proteases have been reported to be powerful catalysts for chemoselective esterification of carbohydrates.[9−11] A variety of sugar-based polymers were synthesized via enzymatic esterification of carbohydrates.[12] As well, polymers of the carbohydrate vinyl esters were reported to indicate the high biodegradability in soil.[13] To the best of our knowledge, however, there has been no paper on the synthesis of sugar derivatives using esterases for biomaterials exhibiting biological recognition activity. In this work, we investigated a facile synthesis of a glycoconjugate polymer via enzyme-catalyzed reaction, the lectin recognition ability, the cell adhension ability, and biodegradability. Our interest in enzymatic chemoselective esterification is its application to the synthesis of biomaterials exhibiting strong binding to specific lectins, which is essential for its application as a scaffold and drug delivery system with recognition ability to cells.

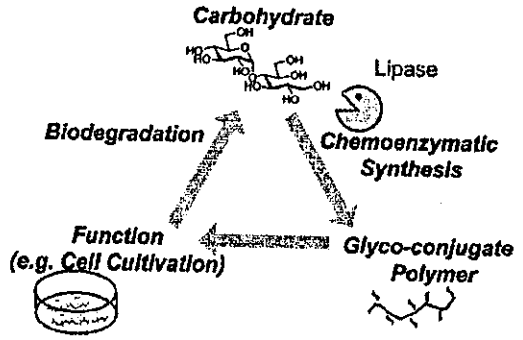


**Figure 1.** Schematic illustration of biomaterial via chemoenzymatic synthesis.

Sugar alcohols (maltitol and lactitol) were chosen as the target carbohydrate, and divinyl sebacate as an acyl donor. Since D-glucitol has been reported to show high reactivity and selectivity, the sugar alcohols are expected to show high enzymatic activity.[14] The open-chain D-glucitol moiety in maltitol might be more reactive than the α-D-Glc unit due to the less steric hindrance, and then the product modified at the D-glucitol moiety could be applicable as a starting substance to lead to a glycoconjugate polymer carrying pendant carbohydrate (Scheme 1).

## Experimental Section

**Materials.** The following reagents were used as received. L-ascorbic acid, *N,N*-dimethylformamide (DMF), dimethyl sulfoxide (DMSO), methanol, pyridine (Kishida, Osaka),

* Corresponding author. Telephone: +81−52−789−2538. Fax: +81−52−789−2528. E-mail: miuray@mol.nagoya-u.ac.jp.

† Abbreviations: AAPD, 2,2′-azobis(2−amidinopropane) dihydrochloride; As-A, *L*-ascorbic acid; ASGPR, asialoglycoprotein receptor; ConA, concanavalin A; DMF, *N,N*-dimethylformamide; BOD, biochemical oxygen demand; DMSO, dimethyl sulfoxide; EDTA, ethylenediaminetetraacetic acid; EMEM, Eagle's minimum essential medium; FAB, fast atom bombardment; Gal, galactose; Glc, glucose; NaPyr, sodium pyruvate; NEAA, nonessential amino acids; PVA, poly(vinyl alcohol); $RCA_{120}$, *Ricinus communis* agglutinin 120; SEC, size exclusion chromatography; TLC, thin-layer chromatography; TOD, theoretical oxygen demand.

10.1021/bm025714b CCC: $25.00 
Published on Web 00/00/0000 PAGE EST: 5.3

**Scheme 1.** Synthesis of Glycoconjugate Polymers via Enzymatic Esterification of Sugar Alcohol and the Subsequent Radical Polymerization[a]

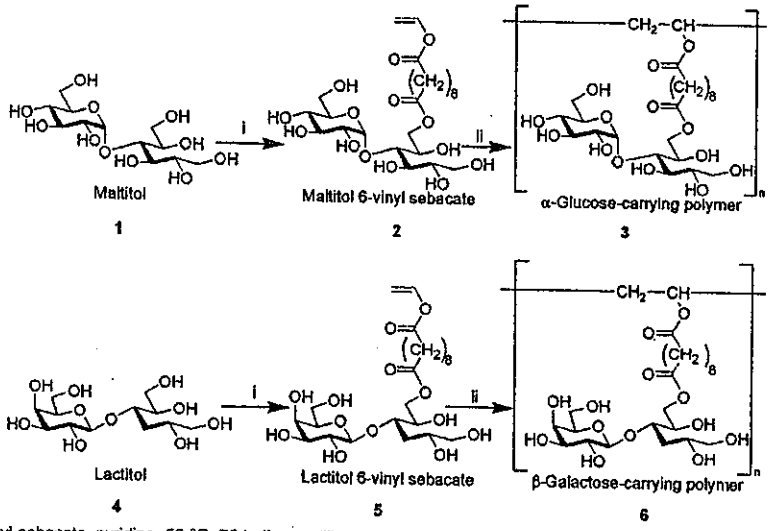


[a] Conditions: (i) divinyl sebacate, pyridine, 50 °C, 72 h, lipase; (ii) radical initiator (AAPD or $H_2O_2$ and *L*-ascorbic acid), $H_2O$/DMSO.

concanavalin A (ConA), *Ricinus communis* agglutinin 120 ($RCA_{120}$) (Honen Co. Ltd., Tokyo), 2,2′-azobis(2−amidinopropane)dihydrochloride (AAPD) (Wako, Osaka), 32% hydrogen peroxide (Mitsubishi Gas Chemical, Tokyo), maltitol (Tokyo Kasei, Tokyo), and lactitol monohydrate (Sigma-Aldrich, Louisiana, MO). The solvent for enzymatic esterification was dried by molecular sieve (4 Å) at least 24 h. Lipases from *Pseudomonas fluorescens* (AK), *Candida rugosa* (AY), and *Pseudomonas cepacia* (PS) were gifts from Amano Enzyme Inc. (Nagoya). The lipase from *Candida antarctica* (CA) was kindly donated by Novo Nordisk Bioindustry Ltd. The lipase from *Porcine pancreas* (PP) was purchased from Sigma-Aldrich. The lipase from *Rhizomucor miehei* (RM) was perchased from Fluka (Buchs, Switzerland).

**Characterizations.** $^1H$ (500 MHz) and $^{13}C$ (125 MHz) NMR spectra were recorded on a Varian Inova 500 equipped with a Sun workstation. The spectra were measured in a mixture of DMSO-$d_6$ and $D_2O$ (100/1, v/v). FTIR spectra were recorded in the form of a KBr disk using a JASCO FT/IR-230. FAB mass spectra were obtained by a JEOL-JMS-AX505HA mass spectrometer using nitrobenzyl alcohol as a matrix. Fluorescence spectroscopy was carried out on a JASCO FP-777 spectrometer at 25 °C. Size exclusion chromatography (SEC) was conducted with JASCO 800 high-performance liquid chromatography on Shodex B804+B805 columns with PBS as an eluent. The molecular weights were estimated using a pullulan standard. The static contact angles of water on the prepared surfaces were measured at 25 °C operating a contact angle goniometer of Face contact-angle meter CA-D (Kyowa Interface Science Co. Ltd., Asaka, Japan).

**Preparation of the Sugar Vinyl Esters.** Enzyme screening was carried out with a Chemistation (EYELA, Tokyo). A mixture of 52 mg of maltitol or 54 mg of lactitol monohydrate (0.15 mmol), 0.15 g of divinyl sebacate (0.60 mmol), and 50 mg of enzyme in 1 mL of pyridine was gently stirred at 50 °C for 72 h. The conversion of sugar alcohol was estimated by high performance liquid chromatography (HPLC) on an Amide 80 column (Tosoh Co. Ltd., Kawasaki, Japan) with an eluent of acetonitrile: water: methanol (8/1/1, v/v/v), and by thin-layer chromatography (TLC). The larger-scale reaction was carried out with 0.52 g of maltitol or 0.54 g of lactitol (1.5 mmol) and 1.5 g of divinyl sebacate (6.0 mmol) in 10 mL of pyridine at 50 °C for 72 h.

**Lectin Recognition Assay.** Immunodiffusion was carried out with agarose, poly(ethylene glycol) and sodium azide in PBS buffer solution by the previous method.[15] The samples were allowed to diffuse for 72 h at room temperature to develop precipitation bands. Binding constants of the glycoconjugates with FITC-labeled lectins were evaluated by the Scatchard plots of the fluorescence spectroscopy.

**Cell Adhesion Assay.** HepG2 cell culture was carried out in EMEM supplemented with 10% fetal bovine serum, 1% NEAA, 1% NaPyr, 100 mU/mL of penicillin, and streptomycin. The surface of polystyrene dishes was treated with an aqueous solution of 1.0 mg/mL the glycoconjugate polymer prior to cell assay.[7b] The cell adhension assay was performed according to the method reported by Donati et al.[7b,16] Confluent cultures of HepG2 cells were detached using 0.025% trypsin and 0.02% EDTA and then suspended in EMEM. A hundred thousand cells were transferred into the polymer-coated polystyrene dishes and incubated at 37 °C. Nonadherent cells were removed by rinsing the dishes with PBS. Cells were then stained with 0.25% CBB (Brilliant Blue G) solution ($H_2O$/acetic acid/ethanol, 9/2/9, v/v/v), and rinsed with PBS. The number of cells was counted by optical microscopy.

**Biochemical Oxygen Demand (BOD) Test.** BOD was determined with a BOD tester (model 200F; TAITEC,

**Table 1.** Enzyme Screen for Esterification of Sugar Alcohols in Pyridine

| enzyme | conversion (%)[a] maltitol | lactitol |
|---|---|---|
| lipase AK | 1 | 93 |
| lipase AY | 0 | 0 |
| lipase CA | 44 | 99 |
| lipase RM | 21 | 15 |
| lipase PS | 0 | 13 |
| lipase PP | 5 | 4 |

[a] HPLC.

Koshigaya, Japan) by the oxygen consumption method, basically according to the JIS standard guidelines (JIS K 6950) at 25 °C using an activated sludge obtained from Nagoya municipal sewage treatment plant in Nagoya City, Japan.

## Results and Discussion

**Monomer Synthesis.** Vinyl esters of carbohydrates can function as monomers of glycoconjugate polymers with poly(vinyl alcohol) backbone.[13] A total of six lipases (lipases AK, AY, CA, RM, PP, and PS) were screened for their capability to catalyze esterification of sugar alcohols (maltitol and lactitol) in pyridine. In both cases, no reaction occurred in the absence of enzyme. The conversion of sugar alcohol and chemoselectivity in esterification were estimated by HPLC and TLC. The results are summarized in Table 1. The conversion of sugar alcohols was modest with most of the enzymes. The lipases were more active in nonpolar solvent,[17,18] which is inapplicable to oligosaccharides due to the lack of solubility.

The conversion of lactitol was much higher than that of maltitol. The high conversion of lactitol is supposed to come from the hydration of lactitol (lactitol monohydrate is used), which might be advantageous to retain the activity of the enzymes.[18] In addition, the hydrophobicity of α-anomeric surface in the galactose moiety might be more preferable than glucose as a substrate. The best lipase was lipase CA.

In lactitol and maltitol, there are eight hydroxyl groups, thereby requiring chemoselective esterification prior to use as monomers. To that end, larger-scale reactions were performed with lipase CA. The resultant compound was purified by the column chromatography, and the chemoselectivity was confirmed by $^{13}C$ NMR, in which the chemical shifts of esterified carbons have been reported to show a downfield shift.[9,19] In the $^{13}C$ NMR of maltitol, three peaks were observed at $\delta$ 61.6, 63.5, and 63.9 ppm due to the primary hydroxymethylenes at the 6′, 1, and 6 positions, respectively. In the $^{13}C$ NMR of the resultant product with lipase CA, the methylene group at the C6 position alone was shifted to a lower magnetic field ($\delta$ 66.7 ppm), indicating that the chemoselective esterification proceeded (Figure 2). The disubstituted compound was not obtained with lipases.[20] The chemoselectivity of lactitol was also confirmed by the same method.[21]

The enzymatic esterification of polyol was reported to be affected by the steric hindrance around the hydroxyl group, and the substitutions of the primary and secondary alcohols

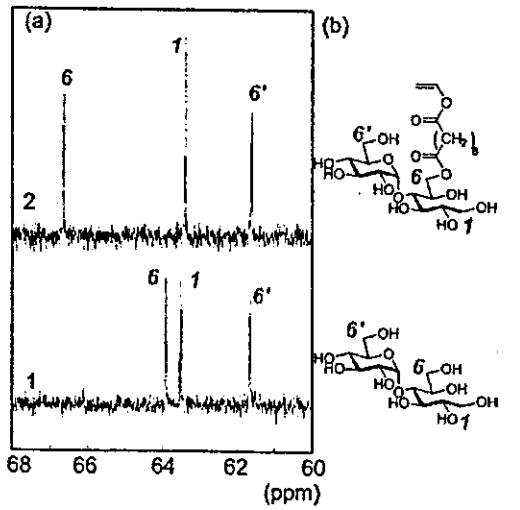


**Figure 2.** (a) Expanded $^{13}C$ NMR of the esterified maltitol by lipase CA (top) and maltitol (bottom) and (b) corresponding chemical structures.

are remarkably discriminated.[22] Glucitol has an open-chain structure and the hydroxyl groups at C1 and C6 are highly reactive with lipases. In the case of maltitol and lactitol, lipase CA showed an outstanding selectivity to the hydroxyl group at the C6 position, but not to that at the C1 position.

**Polymerization of Sugar Alcohol Esters.** The resultant vinyl esters of the sugar alcohols (**2** and **5**) were polymerized by a free radical initiator using 2,2′-azobis(2−amidinopropane) dihydrochloride (AAPD) or hydrogen peroxide with L-ascorbic acid (As-A).[23] The results of the polymerization are summarized in Table 2. The monomers have an amphiphilic structure with longer alkyl chains, and the solubility was poor in many solvents, which made polymerization difficult. **2** was soluble only in water and DMSO, and **5** was soluble a little only in DMSO. Suspension polymerization of **2** proceeded in water with AAPD and hydrogen peroxide/As-A. Suspension polymerization of **5** proceeded in a mixture of water and DMSO only with hydrogen peroxide/As-A. Despite insolubility of monomers, the resulting polymers, **3** and **6**, were readily soluble in water, suggesting the glycocluster formation due to the amphiphilic structure composed of sebacate and carbohydrate.[8] Their molecular weights were on the order of $10^4$. The polymers obtained with hydrogen peroxide/As-A (run nos. 4 and 10 in Table 2) were used in the biological assay.

**Lectin Recognition Ability.** To evaluate the biological ability of the polymers (**3** and **6**), we investigated the affinities with lectins by means of the two-dimensional immunodiffusion test in agar and fluorescence spectrometry (Table 3).

Two-dimensional immunodiffusion tests were carried out using ConA (α-Glc binding lectin) and $RCA_{120}$ (β-Gal binding lectin). Sharp precipitation bands appeared on the gel between ConA and **3** and between $RCA_{120}$ and **6**. Other combinations did not show any precipitation bands, which indicates the specific interactions of glycopolymers with lectins. In addition, sugar alcohols and monomers did not show any bands, indicative of the glyco-cluster effects.

Table 2. Polymerization of Maltitol 6-Vinyl Sebacate (2) and Lactitol 6-Vinyl Sebacate (5)[a]

| run no. | monomer | solvent (mL) $H_2O$/DMSO | AAPD[b] (mol %) | $H_2O_2$ (%) | As-A[c] (mM) | yield (%) | $M_n$ ($\times 10^{-4}$) | $M_w/M_n$ |
|---|---|---|---|---|---|---|---|---|
| 1[d] | 2 | 0.11/0.0 | 1.0 | | | >99 | 1.5 | 3.2 |
| 2[d] | 2 | 0.12/0.10 | 1.0 | | | 54 | 0.69 | 1.6 |
| 3[e] | 2 | 0.0/0.20 | 1.0 | | | 0 | | |
| 4[e] | 2 | 0.20/0 | | 0.032 | 10 | 35 | 2.8 | 2.6 |
| 5[d] | 2 | 0.0/0.20 | | 0.032 | 10 | 0 | | 0 |
| 6[d] | 5[f] | 0.20/0.0 | 1.0 | | | 0 | | |
| 7[b] | 5[f] | 0.10/0.10 | 1.0 | | | 0 | | |
| 8[b] | 5[f] | 0.0/0.20 | 1.0 | | | 0 | | |
| 9[e] | 5[f] | 0.20/0.0 | | 0.032 | 10 | 49 | 2.0 | 1.9 |
| 10[e] | 5[f] | 0.10/0.10 | | 0.032 | 10 | 82 | 1.3 | 1.7 |
| 11[e] | 5[f] | 0.0/0.20 | | 0.032 | 10 | 0 | | |

[a] 10 mg of monomer. [b] 2,2′-Azobis(2-amidinopropane) dihydrochloride. [c] L-Ascorbic acid. [d] Temperature: 60 °C. Time: 20 h. [e] Temperature: 35 °C. Time: 2.5 h. [f] Suspension polymerization.

Table 3. Estimation of Lectin Recognition Abilities

| | immunodiffusion[a] | | affinity constant ($M^{-1}$)[b,c] | |
|---|---|---|---|---|
| | conA | $RCA_{120}$ | conA | $RCA_{120}$ |
| 1 | − | − | $2.1 \times 10^3$ | n.d. |
| 3[d] | + | − | $7.0 \times 10^4$ | n.d. |
| 4 | − | − | n.d. | $1.4 \times 10^3$ |
| 6[e] | − | + | n.d. | $6.1 \times 10^4$ |
| PVLA[f] | − | + | n.d. | $1.3 \times 10^5$ |

[a] The appearance of a precipitation band is shown by (+), and no precipitation band, by (−). [b] The affinity constants are based on the molarity of the glycosyl unit. [c] "n.d."means "not detectable". [d] α-Glc polymer run no. 4 in Table 2. [e] β-Gal polymer run no. 10 in Table 2. [f] $M_n = 5.9 \times 10^4$; $M_w/M_n = 1.7$.

Lectins were precipitated through specific cross-linking with carbohydrate ligands along the polymer chain. The results showed the specific and strong interaction of the polymers (**3** and **6**) with the corresponding lectins.

The binding affinities of the polymers for the lectins were investigated by fluorescent spectroscopy using FITC-labeled lectins (Figure 3). The fluorescence was decreased with the addition of these polymers. The relative change in the fluorescent intensity ($\Delta F/F_o$) at 518 nm was plotted against the carbohydrate concentration. The association constants were estimated by the Scatchard plot as follows:

$$\frac{[\alpha\text{-Glc or }\beta\text{-Gal}]F_o}{\Delta F} = \frac{[\alpha\text{-Glc or }\beta\text{-Gal}]F_o}{\Delta F_{max}} + \frac{F_o}{\Delta F_{max}K_a}$$

where [α-Glc], [β-Gal], $K_a$, $F_o$, $\Delta F$, and $\Delta F_{max}$ represent the concentration of the α-Glc solution (M), the concentration of the β-Gal solution (M), the association constant ($M^{-1}$), the initial fluorescent intensity, the fluorescent change, and the maximum fluorescent change, respectively.

**3** and **6** showed specific affinities to ConA and $RCA_{120}$, respectively, and the affinity constants were much higher than those for the sugar alcohols, indicating again the glycocluster effect. Interestingly, the affinities of sugar alcohols were very weak though they have molecular regognition unit. Though the affinities of **6** to $RCA_{120}$ was lower than that of polystyrene type of glycoconjugate polymer (PVLA: as control) (Figure 4),[7] the neoglyoconjugates with PVA backbone (**6**) showed strong interactions with lectins, and have a potential to application for biomaterials.

**Cell Adhesion Assay.** Prior to the cell adhension assay, polystyrene dishes were treated with aqueous solutions of

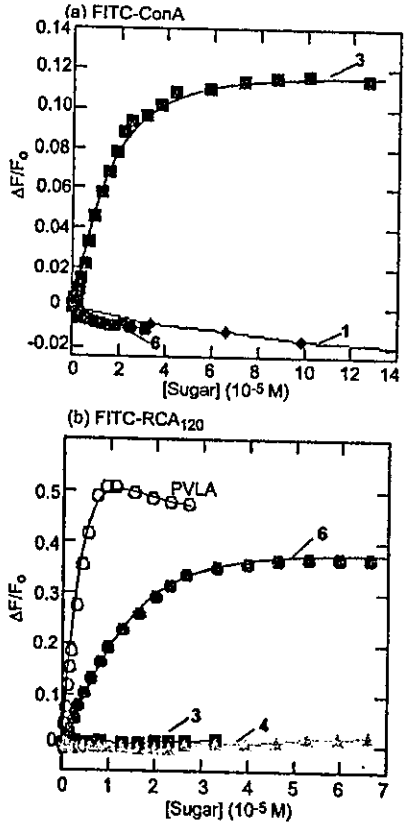


**Figure 3.** Fluorescence intensity changes of FITC-labeled lectins with varying sugar concentration. (a) ConA and (b) $RCA_{120}$.

glycoconjugate polymers. Because of the amphiphilic structure, the glycopolymers could be adsorbed to polystyrene dishes by hydrophobic interaction. The adsorption of glycopolymers onto polystyrene was confirmed by the decrease of the contact angles of the surface (Table 4).

As shown in Figure 5, a **6**-coated polystyrene dish stimulated the adhension of HepG2 more effectively than **3**-coated and noncoated polystyrene dishes. These results suggest that the asialoglycoprotein receptor (ASGPR) plays a key role as a scaffold of hepatocytes on **6**-coated dishes, in contrast to nonspecific interaction of hepatocytes on the other dishes.[7b,16]

# Micropatterned Carbohydrate Displays by Self-Assembly of Glycoconjugate Polymers on Hydrophobic Templates on Silicon

Yoshiko Miura,*,† Hajime Sato,† Takayasu Ikeda,† Hiroyuki Sugimura,‡ Osamu Takai,‡ and Kazukiyo Kobayashi†

*Department of Molecular Design and Engineering and Department of Materials Processing Engineering, Graduate School of Engineering, Nagoya University, Furo-cho, Chikusa-ku, Nagoya 464-8603, Japan*

*Received February 16, 2004; Revised Manuscript Received June 5, 2004*

We report a novel strategy for micropatterned carbohydrate displays on Si substrates. This method exploited the hydrophobic−hydrophilic microfabrication by photolithography of ODS-SAM on Si substrates and the subsequent selective self-assembly of glycoconjugate polymers onto the hydrophobic regions. Protein micropatterning by molecular recognition on the carbohydrate substrates was also successful.

## Introduction

Micropatterned biomacromolecules on solid surfaces have been fabricated for a variety of applications to support the progress of biotechnology. For instance, micropatterned DNAs are extensively used to analyze a vast amount of genes simultaneously.[1,2] Micropatterned proteins are exploited for cell cultivation and biosensors.[3,4] Micropatterned carbohydrates on solid surfaces are expected to analyze carbohydrate−protein interactions and to fabricate the scaffolds of cell cultivation,[5−8] because carbohydrates on cell surfaces play important roles in numerous intercellular recognition processes.[9] Since carbohydrate−protein interactions are usually weak and amplified with multivalent effects,[10] it is important to exploit a strategy for micropatterning of carbohydrate on solid surfaces with the multivalency.

Both "bottom-up" (self-assembly of molecules) and "top-down" (lithography of substrates) processes have been developed to fabricate micropatterned biomolecules on solid surfaces. Self-assembled monolayers (SAMs) on surfaces are paid attention for fabrication of nanomaterials due to their well-defined structures[11] and applicabilities.[12,13] Photolithography of substrate is most practical among various patterning methods and has been applied to the development of microdevices such as electronic circuits and microelectromechanical systems (MEMS), since it can transfer an entire pattern to substrates through a photomask.[14] Combinations of the self-assembly of molecules and lithography of substrates are promising methods for fabricating microstructures on solid surfaces.[15,16]

In this paper, micropatterned displays of carbohydrates on silicon surfaces have been accomplished by a combination of "bottom-up" and "top-down" approaches according to the process illustrated in Figure 1. Here, the well-ordered SAM of octadecyltrimethoxysilane (ODS) on silicon substrates was micropatterned by photolithography using vacuum ultraviolet (VUV) light. Since VUV light of 172 nm wavelength excites and decomposes C−C and C−H bonds, all organic molecules are able to be micropatterned by the photolithography of VUV light.[14] The well-defined hydrophobic−hydrophilic

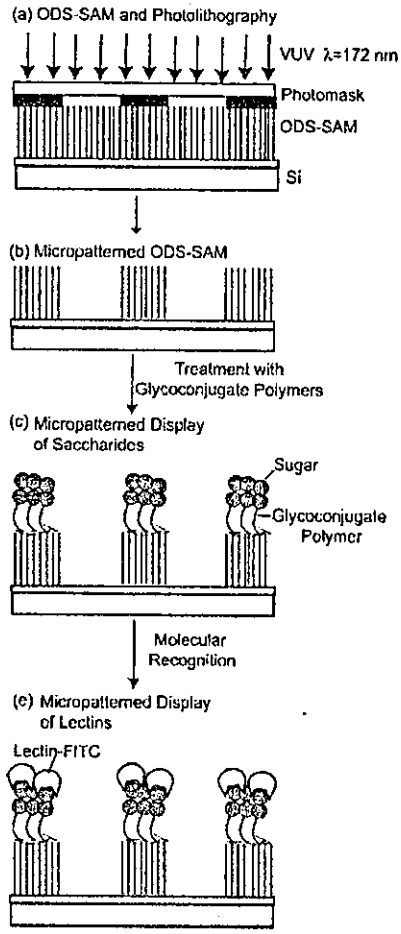


**Figure 1.** Schematic illustration of micropatterned display: (a) photolithography on ODS-SAM, (b) micropatterned ODS-SAM, (c) micropatterned display of carbohydrate, and (d) micropatterned display of lectin.

* To whom correspondence should be addressed. Telephone: +81-52-789-2538. Fax: +81-52-789-2528. E-mail: miuray@mol.nagoya-u.ac.jp.
† Department of Molecular Design and Engineering.
‡ Department of Materials Processing Engineering.

10.1021/bm049904t CCC: $25.00 
Published on Web 00/00/0000 PAGE EST: 5.7

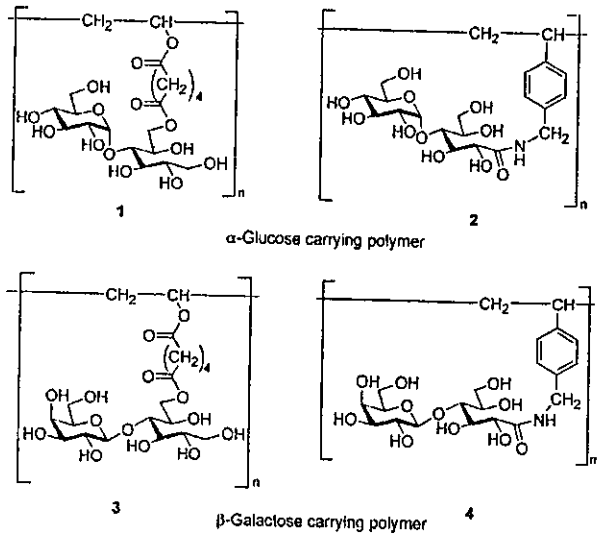


**Figure 2.** Molecular structures of the glycoconjugate polymers.

micropattern was modified by self-assembly of amphiphilic glycoconjugate polymers, and the micropatterned carbohydrate display was visualized by molecular recognition of lectins with fluorescein isothiocyanate (FITC) fluorophore.[17]

Glycoconjugate polymers, each carrying α-Glc (**1** and **2**) and β-Gal (**3** and **4**) as recognition signals, were employed in this paper (Figure 2).[18] Hydrophilic carbohydrate residues are attached to every repeating unit along the hydrophobic polymer backbones (poly(vinyl alcohol) and polystyrene). Owing to the amphiphilic characters, these polymers take characteristic conformations in water and also they are strongly adsorbed to hydrophobic solid surfaces.[19] It is also important that the highly concentrated or clustered carbohydrate residues serve as strong recognition signals to express a variety of biological functions. In addition to these characteristics, the glycopolyvinyl sebacates (**1** and **3**) were biodegradable.

## Experimental Section

**Materials.** Glycoconjugate polymers were synthesized following our previous methods (**1**: $M_n = 0.80 \times 10^4$, $M_w/M_n = 1.7$; **2**: $M_n = 1.0 \times 10^4$, $M_w/M_n = 1.4$; **3**: $M_n = 1.5 \times 10^4$, $M_w/M_n = 1.8$; **4**, $M_n = 1.7 \times 10^4$, $M_w/M_n = 2.4$).[18,20] Concanavalin A (Con A; α-Glc binding lectin), *Ricinus communis* agglutinin 120 ($RCA_{120}$; β-Gal binding lectin) (Honen Co. Ltd., Tokyo), and bovine serum albumin (BSA) (Amersham Bioscience, Uppsala, Sweden) were used as received.

**Measurements.** The static contact angle of water on the prepared surfaces was measured at 25 °C by operating a drop shape analysis system of DSA 10 Mr2 (Krüss, Germany). The thickness of the film on Si(100) substrate was measured with a PZ2000 ellipsometer (Philips, Holland) using a He–Ne laser of 632.8 nm, in which the incident angle was 70° from the normal. The FTIR spectra in the transmission method under a $N_2$ atmosphere were recorded with an FTIR 7000 (Digilab Laboratories, USA) with 1000 times of interferogram accumulation. The surface plasmon resonance (SPR) measurements were performed with a SPR 670 (Nippon Laser & Electronics Labs, Japan). Fluorescence spectroscopy was carried out on a JASCO FP-777 spectrometer at 25 °C. XPS analysis was performed using an ESCA-3300 (Shimadzu/Kratos, Kyoto, Japan) with a collection angle of 45° from the normal. Scanning electron microscopy (SEM) was performed with a JSM-6330F (JEOL Ltd., Japan). Fluorescence microscopic studies were performed using a Zeiss Axiover 200 M laser confocal microscope (Carl Zeiss Inc., Germany) equipped with external argon laser (for excitation at 490 nm).

**Preparation and Photolithgraphy of ODS-SAM.**[14,15] Well-defined ODS-SAM was prepared by the chemical vapor deposition (CVD) method. A silicon substrate was cleaned by UV/ozone irradiation. The cleaned silicon substrate and a glass cup containing ODS liquid were placed in a Teflon container. The container was sealed with a cap and heated in an oven at 150 °C for 4 h. ODS was vaporized and allowed to react with silanol groups on the substrate surface to give ODS-SAM. Formation of ODS-SAM was confirmed by the increase of contact angle from 0° to 103.8°, and the thickness estimated by ellipsometry was 15 Å.

Micropatterned SAM samples were prepared by photolithography. A selected region of ODS-SAM was photochemically decomposed and removed by irradiation with VUV light (excimer lamp, Ushio Inc., UER20-172V, $\lambda$ = 172 nm and 10 mW/cm$^2$) through a photomask under a reduced pressure of 10 Pa for 30 min.

**Glycoengineering and Lectin Binding on the Micropatterned Surface.** The patterned ODS-SAM substrates were incubated in an aqueous solution of the glycoconjugate polymers (**1**–**4**) (0.5 mg/mL) at room temperature for 5 h. The substrate was rinsed thoroughly with distilled water and dried in a stream of nitrogen gas and under vacuum. The resultant polymer-coated substrate was incubated with FITC-labeled lectin (Con A and $RCA_{120}$) in 1 mg/mL phosphate-buffered saline (PBS) solution at room temperature for 2 h, and then washed with PBS to remove weakly bound substance. The fluorescence image was recorded with a fluorescence microscope and analyzed with Scion image software (version 4.02 beta, Scion Co., Frederick, MD).

**Lectin Recognition Assay.** The binding constants of the glycoconjugate polymers with lectins were evaluated on substrates by surface plasmon resonance and in aqueous solutions by fluorescence spectroscopy.

To evaluate the lectin recognition ability on substrates, surface plasmon resonance (SPR) measurements were performed at 25 °C with a flow rate of 15 μL/min, in which SAM of octadecylmercaptan on gold was used instead of ODS-SAM, and the glycoconjugate polymers were adsorbed on the SAM to evaluate the binding constants on the substrates. Kinetic and binding constants were calculated from the sensorgrams with SPR software (SPR Processing, version 4.00, Nippon Laser & Electronics Labs). Langmuir binding between the glycopolymer and lectin (glycopolymer + lectin → glycopolymer–lectin) was assumed in the calculation. The glycopolymer-coated substrate was used as the control in SPR analysis.

In an aqueous solution, the relative change of the fluorescent intensity ($\Delta F/F_0$) at 518 nm was plotted against

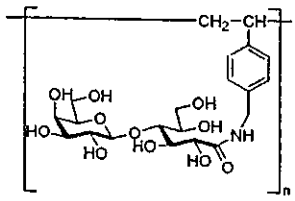

PVLA

Figure 4. Lactose-carrying polystyrene (PVLA).

Table 4. Contact Angles of the Polymer Coated Dishes[a]

| polymer | contact angle (deg) |
|---|---|
| 3 | 60 |
| 6 | 61 |
| polystyrene (control) | 75 |

[a] The polystyrene dishes were treated with the glycoconjugate polymer solution of 1.0 mg/mL for 13 h.

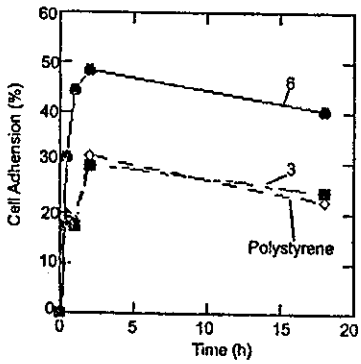


Figure 5. Cell adhension efficiency on the polymer coated dishes.

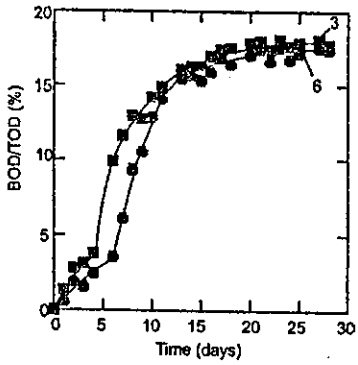


Figure 6. Biodegradability of the glyco-conjugate polymers (3 and 6) with PVA backbone.

**Biodegradability.** These glycoconjugate polymers consist of biodegradable dicarboxylic ester of PVA, and carbohydrates. The biodegradability of the polymers was evaluated by the biochemical oxygen demand (BOD)/theoretical oxygen demand (TOD) value using the oxygen consumption method (Figure 6).

The biodegradabilities of **3** and **6** were modest, but much improved from PVA (less than 5%).[13,24] Figure 7 is the FTIR spectra of **3** and **6** before and after the degradation. The strong adsorption of alkyl chain and ester bond around 2950

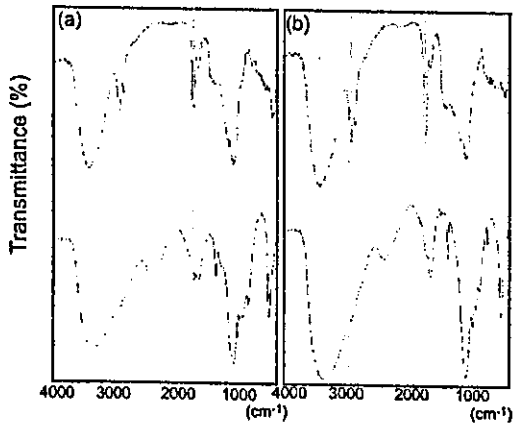


Figure 7. FTIR spectra of (a) 3 and (b) 6 before (top) and after (bottom) biodegradation.

and 1730 $cm^{-1}$ decreased after biodegradation, which suggests that pendant carboxylic acid and sugar alcohol moieties are degraded with preference. The biodegradability of **3** and **6** implies that these glycoconjugate polymers are useful not only as biomaterials but also as green materials which can be regarded as a chemical recycling system for biomaterials.

## Conclusion

Novel glycoconjugate polymers were synthesized via a facile chemoenzymatic reaction. The lipase catalyzed esterification of sugar alcohols (maltitol and lactitol) with divinyl sebacate provided sugar vinyl ester. With lipase from *C. antarctica*, maltitol 6-vinyl ester and lactitol 6-vinyl ester were obtained at high yield and chemoselectivity. The sugar vinyl esters were successfully polymerized into glycoconjugate polymers of poly(vinyl alcohol) derivatives with hydrogen peroxide and L-ascorbic acid initiator. The glycoconjugate polymers showed strong and specific interactions with lectins and hepatocytes due to the multivalency. The biodegradability of the gycoconjugate polymers were modest but higher than PVA. It is important to note that the chemoenzymatic synthesis can be a new method for biomaterial fabrication.

**Acknowledgment.** This work was supported by a Grant-in-Aid for Young Scientist (B) and by the Japan Chemical Innovation Institute (JCII), Hattori-Hokokai Foundation, Sekisui Integrated Research Foundation, and Eno Science Foundation. The authors are grateful to Prof. Shiro Kobayashi, and Prof. Hiroshi Uyama (Kyoto University) for helpful discussion on enzymatic synthesis, to Dr. Yoshihiro Ito (Kanagawa Academy of Science and Technology) for helpful support on the biological assay, and to Prof. Keigo Aoi (Nagoya University) for helpful support on the BOD experiment.

**Supporting Information Available.** Text giving characterization information and spectral data for **2** and **5**, and a figure showing the expanded $^{13}C$ NMR spectra of **4** and **5** for estimation of chemoselectivity. This material is available free of charge via the Internet at http://pubs.acs.org.

## References and Notes


(1) Varki, A. *Glycobiology* **1993**, *3*, 97.
(2) For example: Lee, R. T.; Ichikawa, Y.; Fay, M.; Drickamer, K.; Shao, M. C.; Lee, Y. C. *J. Biol. Chem.* **1991**, *266*, 4810.
(3) Lee, Y. C. *Carbohydr. Res.* **1978**, *67*, 509.
(4) (a) Lee, R. T.; Lee, Y. C. *Neoglycoconjugates: Preparations and Applications*: Lee, Y. C., Lee, R. T., Eds.; Academic: San Diego, CA, 1994; pp 23−50. (b) Lee, Y. C.; Lee, R. T. *Acc. Chem. Res.* **1995**, *28*, 321.
(5) Lainé, V.; Coste-Sarguet, A.; Gadelle, A.; Defaye, J.; Perly, B.; Djudami-Pilard, F. *J. Chem. Soc., Perkin Trans. 2* **1995**, *11*, 1479.
(6) Roy, R.; Kim, J. M. *Angew. Chem., Int. Ed. Engl.* **1999**, *38*, 369.
(7) (a) Kobayashi, K.; Sumitomo, H.; Ina, Y. *Polym. J.* **1985**, *17*, 567. (b) Kobayasi, A.; Akaike, T.; Kobayashi, K.; Sumitomo, H. *Makromol. Chem., Rapid Commun.* **1986**, *7*, 645. (c) Tsuchida, A.; Kobayashi, K.; Matsubara, N.; Muramatsu, T.; Suzuki, T.; Suzuki, Y. *Glycoconjugate J.* **1998**, *15*, 1047.
(8) Watanoka, I.; Urakawa, H.; Kajiwara, K.; Kobayashi, K. *Macromolecules* **1999**, *32*, 1816.
(9) (a) Therisod, M.; Klibanov, A. M. *J. Am. Chem. Soc.* **1986**, *108*, 5638. (b) Therisod, M.; Klivanov, A. M. *J. Am. Chem. Soc.* **1987**, *109*, 3977. (c) Sergio, R.; Chopineau, J.; Kieboom, A. P. G.; Klibanov, A. M. *J. Am. Chem. Soc.* **1988**, *110*, 584.
(10) Gross, R. A.; Kumar, A.; Karla, B. *Chem. Rev.* **2001**, *101*, 2097.
(11) Kobayashi, S.; Uyama, H.; Kimura, S. *Chem. Rev.* **2001**, *101*, 3793.
(12) Chen, X.; Martin, B. D.; Neubauer, T. K.; Linhardt, R. J.; Dordick, J. S.; Rethwisch, D. G. *Carbohydr. Polym.* **1995**, *28*, 15.
(13) (a) Tokiwa, Y.; Fan, H.; Hiraguri, Y.; Kuraue, R.; Kitagawa, M.; Shibatani, S.; Maekawa, Y. *Macromolecules* **2000**, *33*, 1636. (b) Kitagawa, M.; Tokiwa, Y. *Biotechnol. Lett.* **1998**, *20*, 627.
(14) Uyama, H.; Klegraf, E.; Wada, S.; Kobayashi, S. *Chem. Lett.* **2000**, 800.
(15) Kobayashi, K.; Akaike, T. *Trends Glycosci. Glycotechnol.* **1990**, *2*, 26.
(16) Donati, I.; Gamini, A.; Vetere, A.; Campa, C.; Paoletti, S. *Biomacromolecules* **2002**, *3*, 805.
(17) Klivanov, A. M. *CHEMTECH* **1986**, *16*, 354.
(18) Gorman, L. A. S.; Dordick, J. S. *Biotechnol. Bioeng.* **1992**, *39*, 392.
(19) Yoshimoto, K.; Itatani, Y.; Tsuda, Y. *Chem. Pharm. Bull.* **1980**, *28*, 2065.
(20) Maltitol 6,6′-divinyl sebacate (2%) and lactitol 6,6′-divinyl sebacate (3%) was obtained in the case of protease from *Bacillus sp.*
(21) The analytical data of the compounds are available in the Supporting Information.
(22) Halldorsson, A.; Magnusson, C. D.; Haraldsson, G. G. *Tetrahedron Lett.* **2001**, *42*, 7675.
(23) Larpent, C.; Tadros, T. F. *Colloid Polym. Sci.* **1991**, *269*, 1171.
(24) Takasu, A.; Itou, H.; Takada, Y.; Inai, Y.; Hirabayashi, T. *Polymer* **2002**, *43*, 227.


BM025714B

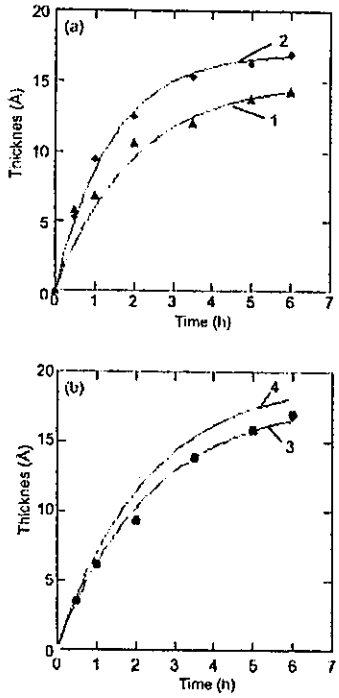


Figure 3. Thicknesses of the glycoconjguate polymers (1–4) of ODS-SAM on Si substrate estimated by ellipsometry: (—) calulation according to Langmuir isotherms.

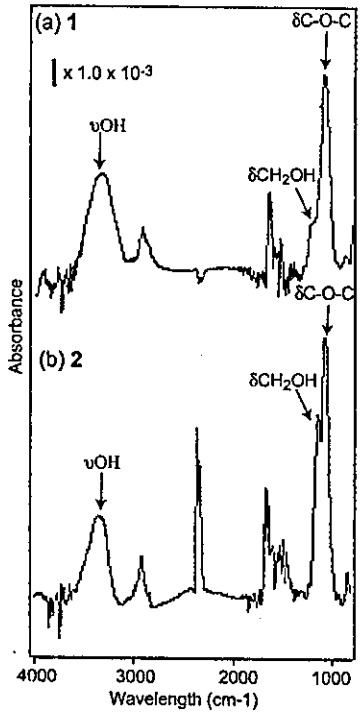


Figure 4. FTIR spectra on Si substrate: (a) 1-coated ODS-SAM and (b) 2-coated ODS-SAM.

the carbohydrate concentration. The association constants were estimated by the Scatchard plot as follows:[20]

$$\frac{[\text{sugar}]F_a}{\Delta F} = \frac{[\text{sugar}]F_o}{\Delta F_{max}} + \frac{F_o}{\Delta F_{max}K_a}$$

where [sugar], $K_a$, $F_o$, $\Delta F$, and $\Delta F_{max}$ represent the concentration of the sugar unit (α-Glc or β-Gal) (M) of the polymer, the association constant ($M^{-1}$), the initial fluorescent intensity, the fluorescent change, and the maximum fluorescent change, respectively.

## Result and Discussion

**Adsorption of the Glycoconjugate Polymers on ODS-SAM.**[21] The adsorption behaviors of the glycoconjugate polymers were studied with ODS-SAM before applying photolithography. Immersing an ODS-SAM substrate in an aqueous solution of glycoconjugate polymer decreased the contact angles on the substrate: unreacted ODS-SAM, 103.8°; treated with **1**, 70.5°; treated with **2**, 78.2°; treated with **3**, 73.8°; treated with **4**, 79.3°. The thicknesses of the polymer layers estimated by ellipsometry were increased with the immersion to reach 15–20 Å after 5–6 h irrespective of the polymer backbones and sugar structures, and the time courses of the polymer adsorption were followed by the Langmuir equation (Figure 3).[22] Typical bands due to carbohydrates of the polymer-coated ODS-SAM on Si were observed by FTIR in Figure 4: $\upsilon$(O–H, broad peak around 3400 $cm^{-1}$), $\delta$($C_6$–O–H around 1250 $cm^{-1}$), and $\delta$(C–O–C, carbohydrate ring, around 1100 $cm^{-1}$).[23] XPS observation of the polymer-coated ODS-SAM is described in a later section. On the other hand, the glycoconjugate polymers were little adsorbed on bare hydrophilic Si. It is suggested that these glycoconjugate polymers were specifically adsorbed on the hydrophobic ODS-SAM by the interaction between the polymer backbone and substrate and that the saccharide moieties of the polymers were exposed to the surface.

**Lectin Recognition on Substrates.** The affinities of Con A and $RCA_{120}$ lectins to the glycopolymer-coated substrates were estimated by SPR (Figure 5). Strong and specific responses of Con A to **1** and **2** and $RCA_{120}$ to **3** and **4** were observed in the SPR shift angles. Typically, the maximum SPR shift angle of Con A to **2** was 7 times that of $RCA_{120}$ to **2** and 50 times that of BSA to **2**. The sensorgrams of **2** and **4** with polystyrene backbone showed a more rapid rise in the association phase and a more rapid downturn in the dissociation phase than those of **1** and **3** with poly(vinyl alcohol) backbone. The association of $RCA_{120}$ to **4** was much faster than that of Con A to **2**. These observations can be evaluated by the kinetic treatments of the sensorgrams, which gave the association and dissociation rate constants ($k_a$ and $k_d$) and association constant ($K_a$) as summarized in Table 1.

Nonspecific interactions $K_a$ ($M^{-1}$) of BSA to the glycopolymer-coated substrates evaluated with the SPR software were weak: **1**, $2.5 \times 10^{-1}$; **2**, $4.1 \times 10^{-1}$; **3**, $1.0 \times 10^{-2}$; **4**, 5.3. On the other hand, nonspecific interactions of the lectins to the octadecylmercapto-SAM were much strong without specificity (Con A, $6.6 \times 10^6$; $RCA_{120}$, $1.1 \times 10^7$; BSA, $8.6 \times 10^5$ ($M^{-1}$)).[24,25]

The specific and strong interactions of the lectins to the polymer-coated substrates can be discussed with respect to the association constants. The glycopolymers with polystyrene backbone were superior in both interaction and specificity to those with poly(vinyl alcohol) backbone. The protein–carbohydrate interactions are affected not only by the

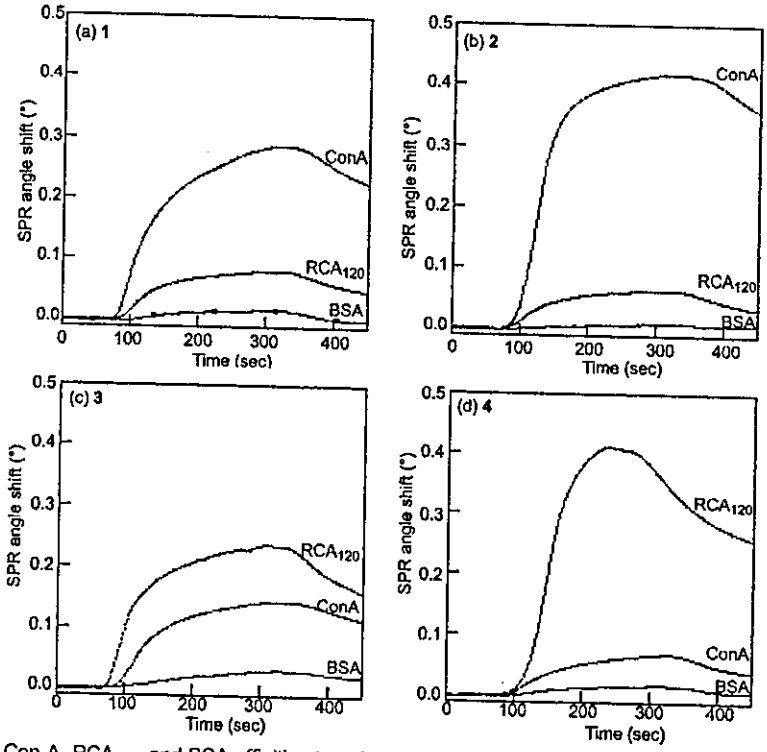


**Figure 5.** SPR analyses of Con A, $RCA_{120}$, and BSA affinities to polymer-coated substrates (1–4) at 25 °C.

**Table 1.** Association and Dissociation Rate Constants and Equilibrium Association Constants of the Polymer-Coated Surfaces to Lectins by SPR

| | Con A | | | $RCA_{120}$ | | |
|---|---|---|---|---|---|---|
| | $k_a$ ($M^{-1}$ $s^{-1}$) | $k_d$ ($s^{-1}$) | $K_a$ ($M^{-1}$) | $k_a$ ($M^{-1}$ $s^{-1}$) | $k_d$ ($s^{-1}$) | $K_a$ ($M^{-1}$)[a] |
| 1 | $1.9 \times 10^3$ | $3.7 \times 10^{-3}$ | $5.2 \times 10^5$ | 10.0 | $6.2 \times 10^{-3}$ | $1.6 \times 10^3$ |
| 2 | $4.7 \times 10^5$ | $1.3 \times 10^{-3}$ | $3.6 \times 10^8$ | 2.3 | $1.1 \times 10^{-2}$ | $2.2 \times 10^2$ |
| 3 | 8.4 | $1.1 \times 10^{-2}$ | $7.6 \times 10^2$ | $1.3 \times 10^3$ | $8.0 \times 10^{-3}$ | $1.6 \times 10^5$ |
| 4 | 5.9 | $1.2 \times 10^{-2}$ | $4.9 \times 10^2$ | $1.7 \times 10^6$ | $3.3 \times 10^{-2}$ | $5.2 \times 10^7$ |

**Table 2.** Association Constants of Glycoconjugate Polymers with Lectins in Aqueous Solution by Fluorescence Spectroscopy

| | $K_a$[a] ($M^{-1}$) | |
|---|---|---|
| | Con A | $RCA_{120}$ |
| maltitol | $1.1 \times 10^3$ | n.d.[b] |
| 1 | $3.6 \times 10^5$ | $9.5 \times 10^3$ |
| 2 | $4.5 \times 10^5$ | $1.4 \times 10^3$ |
| 3 | $7.4 \times 10^3$ | $2.6 \times 10^4$ |
| 4 | $2.4 \times 10^3$ | $1.3 \times 10^5$ |

[a] The affinity constants are based on the molarity of glycosyl unit. [b] n.d., not detectable.

saccharide structures but also by the glyco cluster scaffold. The influence of the glyco scaffold on the lectin recognition has been pointed out by our group[18,26] and other groups.[27,28]

Lectin affinities of the polymers in aqueous solutions were estimated by fluorescence spectroscopy for comparison (Table 2). Specific and strong interactions in aqueous solutions (Con A to **1** and **2**, and $RCA_{120}$ to **3** and **4**) were observed as well as those on the substrate. The affinities were much stronger than those of isolated sugar due to the glyco cluster effects of the polymers. The glycopolymers on the substrate showed stronger interactions with lectins than those in aqueous solution, which indicated the polymer-coated

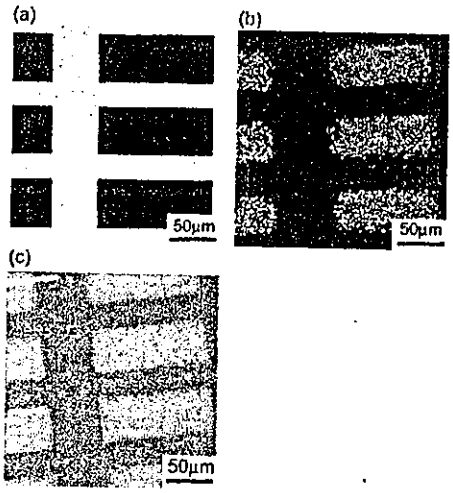


**Figure 6.** Optical micrographs on Si substrate: (a) photomask used and (b) the micropatterned ODS-SAM stained with water vapor. (c) SEM of 1-coated substrate.

substrates maintain and amplify the glyco cluster effects of the polymers.

**Micropatterned Adsorption of Glycoconjugate Polymers.** Hydrophobic–hydrophilic micropatterned ODS-SAM was prepared by photolithography using VUV light at 172 nm. The decomposition of ODS by photoirradiation was confirmed by the decrease of contact angle of the substrate and also visualized by optical micrographs (Figure 6a,b).

Then the micropatterned ODS-SAMs were immersed in aqueous solutions of glycoconjugate polymers. SEM suggests that the glycoconjugate polymer was adsorbed on ODS-SAM region (Figure 6c). The representative XPS spectra of the polymer-coated substrates on the ODS-SAM are shown in Figure 7.[29] The C 1s spectra were resolved by the pseudo-

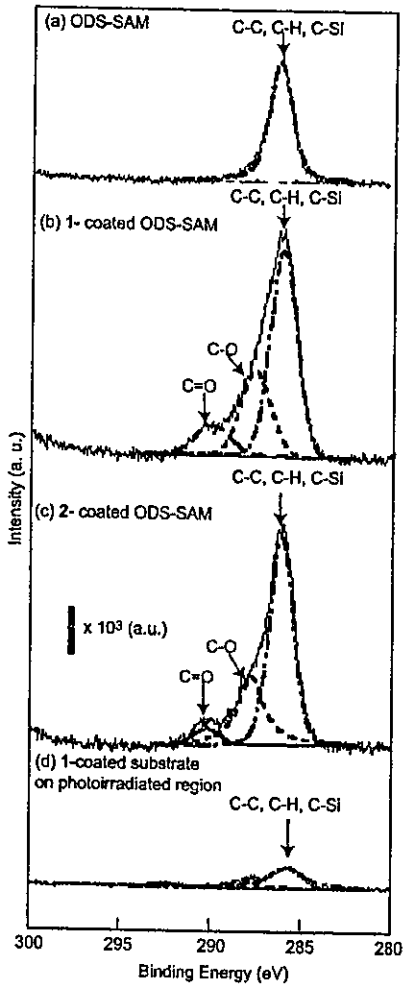


**Figure 7.** XPS spectra on Si substrate: (a) ODS-SAM, (b) **1**-coated ODS-SAM, (c) **2**-coated ODS-SAM, and (d) **1**-coated substrate on photoirradiated region.

Voigt function. In the ODS-SAM (Figure 7a), the main peak around 286.3 eV was assigned to C−C, C−H, and C−Si bands. The polymer-coated ODS-SAM (Figure 7b,c) showed shoulders around 288.5 and 290.5 (eV) in the C 1s region, which corresponded to the C−O of saccharides and esters and C=O of esters and amide of the polymer side chains. On the other hand, the intensities of C−O and C=O peaks on the photodegraded region were almost 10% of those on ODS-SAM (Figure 7d), indicating the selective adsorption of the polymers on the micropatterned substrate.

**Micropatterned Lectin Displays on the Glycoconjugate Polymer Substrates.** The lectin recognition of the micropatterned carbohydrates was visualized by fluorescence microscopy using FITC-labeled lectin (Figure 8). Fluorescence images were observed along the micropatterns, and the patterning was specific to the combination between carbohydrates and lectins (**1** and **2** to Con A, and **3** and **4** to $RCA_{120}$).

The lectin patterning to glycopolymer-coated substrates on ODS-SAM was assessed by XPS and fluorescent intensity.[30] The atomic percentages of N 1s/C 1s were in the range of 0.22−0.30 for the specific combinations of Con A to **1** and **2** on ODS-SAM and of $RCA_{120}$ to **3** and **4** on ODS-SAM. These values were not high enough to be compared

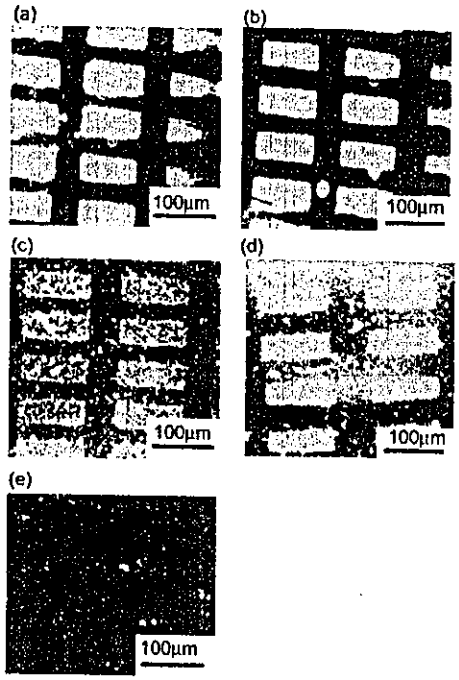


**Figure 8.** Fluorescence micrographs on Si substrate: (a) Con A on **1**-coated ODS-SAM, (b) Con A on **2**-coated ODS-SAM, (c) $RCA_{120}$ on **3**-coated ODS-SAM, (d) $RCA_{120}$ on **4**-coated ODS-SAM (negative pattern), and (e) $RCA_{120}$ on **1**-coated ODS-SAM (discordant combination).

with 0.16 for Con A to **1** on photodegraded ODS. The fluorescent intensity ratios of the micropatterned region to the background photodegraded region were in the range of 1.8−2.3 for the specific combinations. The contrast of patterning of the lectins was not complete, compared to the high contrast or selective adsorption of the glycoconjugate polymers to ODS-SAM as suggested by XPS peak intensity ratio (Figure 7). The shapes of the fluorescence images were also slightly different from each other (Figure 8a−d) due to the nonspecific adsorption of protein. The blocking method is required to attain the better lectin patterning.

Photolithography,[31] microcontact printing,[32] and spotting[33] are well established and utilized for a variety of biomacromolecular micropatternings. However, these micropatternings are affected by substrate properties, photochemical processes, and ambient conditions. The self-assembly of biomacromolecules is another potential approach of patterning to modify the surface properties,[34] and the self-assembly in aqueous solution by hydrophobic interaction and molecular recognition is a universal driving force for formation of microstructures, which applies to a variety of molecules and substrates.

## Conclusions

We have proposed a new method for micropatterned carbohydrate displays, which are achieved by the self-assembling of the glycoconjugate polymers on the hydrophobic micropatterns prepared via photolithography of ODS-SAM. Lectins were also selectively adsorbed on the carbohydrate displays to form micropatterned proteins.

This patterning strategy is based on the self-assembly of biomacromolecules, and is applicable for a variety of

substrates such as ceramics, metals, and polymers. The micropatterning via hydrophobic−hydrophilic templates is useful for the fabrication of micropatterned biomacromolecules and nanomaterials. The combination of the top-down material processing (lithography) and the bottom-up processing (self-assembly of the biomacromolecules) is one of the key methodologies for the nanomaterials. Carbohydrate microchips and patterned cell cultivations using this strategy are currently under way.

**Acknowledgment.** This work was supported by the Industrial Technology Research Grant Program in 2003 from the New Energy and Industrial Technology Development Organization (NEDO) of Japan, and the 21st Century COE Program "Nature-Guided Materials Processing". The authors are grateful to Dr. Yoshihiro Ito and Mr. Hiroshi Makino (Kanagawa Academy of Science and Technology) for helpful support in the fluorescence microscopy experiments, and to Dr. Masamichi Kamihira and Mr. Akio Sakaki (Nagoya University) for SPR measurements.

**Supporting Information Available.** Text giving synthesis of polymer **1**, surface characterizations, and patterning assessments by XPS and fluorescence intensities. This material is available free of charge via the Internet at http://pubs.acs.org.

## References and Notes

(1) Ziauddin, J.; Sabatini, D. M. *Nature* **2001**, *411*, 107.
(2) Lange, S. A.; Benes, V.; Kern, D. P.; Höber, J. K. H.; Bernald, A. *Anal. Chem.* **2004**, *76*, 1641.
(3) Yang, Z.; Frey, W.; Oliver, T.; Chilkoti, A. *Langmuir* **2000**, *16*, 1751.
(4) Mrksich, M.; Whitesides, G. M. *Trends Biotechnol.* **1995**, *13*, 228.
(5) (a) Brayan, M. C.; Plettenburg, O.; Sears, P.; Rebuka, D.; Wacowich-Sgarbi, S.; Wong, C.-H. *Chem. Biol.* **2002**, *9*, 713. (b) Fazio, F.; Bryan, M. C.; Blixt, O.; Paulson, J. C.; Wong, C.-H. *J. Am. Chem. Soc.* **2002**, *124*, 14397.
(6) (a) Houseman, B. T.; Mrksich, M. *Chem. Biol.* **2002**, *9*, 443. (b) Su, J.; Mrksich, M. *Angew. Chem., Int. Ed.* **2002**, *41*, 4715.
(7) Park, S.; Shin, I. *Angew. Chem., Int. Ed.* **2002**, *41*, 3180.
(8) Shirahata, N.; Yonezawa, T.; Miura, Y.; Kobayashi, K.; Kounoto, K. *Langmuir* **2003**, *19*, 9107.
(9) Taylor, M. E.; Kurt, D. *Introduction to Glycobiology*; Oxford University Press: New York, 2003.
(10) Lee, Y. C. *Carbohydr. Res.* **1978**, *67*, 509.
(11) Ulman, A. *An Introduction to Ultrathin Organic Films: From Langmuir-Blodgett to Self-Assembly*; Academic Press: Boston, MA, 1991.
(12) Lee, Y.-S.; Mrksich, M. *Trends Biotechnol.* **2002**, *20*, 14.
(13) Miura, Y.; Sasao, Y.; Dohi, H.; Nishida, Y.; Kobayashi, K. *Anal. Biochem.* **2002**, *310*, 27.
(14) (a) Sugimura, H.; Hanji, T.; Takai, O.; Masuda, T.; Misawa, H. *Electrochim. Acta* **2001**, *47*, 103. (b) Sugimua, H.; Ushiyama, K.; Hozumi, A.; Takai, O. *Langmuir* **2000**, *16*, 885.
(15) Sugimura, H.; Hozumi, A.; Kameyama, T.; Takai, O. *Adv. Mater.* **2001**, *13*, 667.
(16) (a) Sighavi, R.; Kumar, A.; Lopez, G. P.; Stephanolpoulos, G. N.; Wang, D. I.; Whitesides, G. M.; Ingber, D. E. *Science* **1994**, *264*, 696. (b) Xia, Y.; Mrksich, M.; Kim, E.; Whitesides, G. M. *J. Am. Chem. Soc.* **1995**, *117*, 9576. (c) Aizenberg, J.; Black, A. J.; Whitesides, G. M. *Nature* **1999**, *398*, 495.
(17) Sun, X.-L.; Faucher, K. M.; Houston, M.; Grande, D.; Chaikof, E. L. *J. Am. Chem. Soc.* **2002**, *124*, 7258.
(18) (a) Kobayasi, A.; Akaike, T.; Kobayashi, K.; Sumitomo, H. *Makromol. Chem., Rapid Commun.* **1986**, *7*, 645. (b) Miura, Y.; Ikeda, T.; Kobayashi, K. *Biomacromolecules* **2003**, *4*, 410. (c) Miura, Y.; Ikeda, T.; Wada, N.; Sato, H.; Kobayashi, K. *Green Chem.* **2003**, *5*, 610.
(19) Suzuki, N.; Quesenberry, M. S.; Wang, J. K.; Lee, R. T.; Kobayashi, K.; Lee, Y. C. *Anal. Biochem.* **1997**, *247*, 412.
(20) Scatchard, G. *Ann. N.Y. Acad. Sci.* **1949**, *51*, 660.
(21) (a) Matsuura, K.; Tsuchida, A.; Okahata, Y.; Akaike, T.; Kobayashi, K. *Bull. Chem. Soc. Jpn.* **1998**, *71*, 2973. (b) Tsuchida, A.; Matsuura, K.; Kobayashi, K. *Macromol. Chem. Phys.* **2000**, *201*, 2245.
(22) The adsorption of glycoconjugate polymers was reported in ref 21. In the present case, the thicknesses of the adsorbed layers were evaluated after thorough washing and drying under $N_2$.
(23) Revell, D. J.; Knight, J. R.; Blyth, D. J.; Haines, A. H.; Russell, D. A. *Langmuir* **1998**, *14*, 4517.
(24) Prime, K. L.; Whitesides, G. M. *Science* **1991**, *252*, 1164.
(25) Luk, Y.-Y.; Kato, M.; Mrksich, M. *Langmuir* **2000**, *16*, 9604.
(26) Hasegwa, T.; Kondoh, S.; Matsuura, K.; Kobayashi, K. *Macromolecules* **1999**, *32*, 6595.
(27) Gestwicki, J. E.; Cairo, C. W.; Strong, L. E.; Oetjen, K. A.; Kiessling, L. L. *J. Am. Chem. Soc.* **2002**, *124*, 14922.
(28) Lundquist, J. J.; Toone, E. J. *Chem. Rev.* **2002**, *102*, 555.
(29) Kugumiya, T.; Yagawa, A.; Maeda, A.; Nomoto, H.; Tobe, S.; Kobayashi, K.; Matsuda, T.; Onishi, T.; Akaike, T. *J. Bioactive Biocompatible Polym.* **1992**, *7*, 338.
(30) Lee, C.-S.; Lee, S.-H.; Park, S.-S.; Kim, Y.-K.; Kim, B.-G. *Biosens. Bioelectron.* **2003**, *18*, 437.
(31) Ito, Y.; Nogawa, M.; Sugimura, H.; Takai, O. *Langmuir* **2004**, *20*, 4299.
(32) Mrksich, M.; Whitesides, G. M. *Trends Biotechnol.* **1995**, *13*, 228.
(33) Revzin, A.; Rajagopalan, P.; Tilles, A. W.; Berthiaume, F.; Yarmush, M.; Toner, M. *Langmuir* **2004**, *20*, 2999.
(34) Khademhosseini, A.; Suh, K. Y.; Yang, J. M.; Eng, G.; Yeh, J.; Levenberg, S.; Langer, R. *Biomaterials* **2004**, *25*, 3583.

BM049904T

THE JOURNAL OF BIOLOGICAL CHEMISTRY
Vol. 279, No. 32, Issue of August 6, pp. 33281–33289, 2004
Printed in U.S.A.


# A Novel Mechanism for the Inhibition of Hyaluronan Biosynthesis by 4-Methylumbelliferone*

Received for publication, May 27, 2004
Published, JBC Papers in Press, June 9, 2004, DOI 10.1074/jbc.M405918200

**Ikuko Kakizaki‡, Kaoru Kojima‡, Keiichi Takagaki‡, Masahiko Endo‡, Reiji Kannagi§¶, Masaki Ito‖, Yoshihiro Maruo**, Hiroshi Sato‡‡, Tadashi Yasuda§§, Satoka Mita§§¶¶, Koji Kimata§§, and Naoki Itano‡§§‖‖**

*From the ‡Department of Biochemistry, Hirosaki University School of Medicine, 5 Zaifu-cho, Hirosaki 036-8562, §Program of Molecular Pathology, Aichi Cancer Center, Research Institute, Nagoya 464-8681, ¶Core Research for Evolutional Science and Technology, Japan Science and Technology Agency, ‖Second Department of Internal Medicine, the **Department of Pediatrics and the ‡‡Department of Biology, Shiga University of Medical Science, Seta, Otsu, Shiga, the ¶¶Department of Biochemistry, Osaka University Medical School, 2-2 Yamadaoka, Suita, Osaka 565-0871, and §§Institute for Molecular Science of Medicine, Aichi Medical University, Nagakute, Aichi 480-1195, Japan*

**Specific inhibitors of hyaluronan (HA) biosynthesis can be valuable therapeutic agents to prevent cancer invasion and metastasis. We have found previously that 4-methylumbelliferone (MU) inhibits HA synthesis in human skin fibroblasts and in group C *Streptococcus*. In this paper, the inhibition mechanism in mammalian cells was investigated using rat 3Y1 fibroblasts stably expressing HA synthase (HAS) 2. Exposure of the transfectants to the inhibitor resulted in significant reduction of HA biosynthesis and matrix formation. The evaluation of HAS transcripts and analysis of cell-free HA synthesis demonstrated the post-transcriptional suppression of HAS activity by MU. Most interesting, the post-transcriptional suppression of HAS activity was also observed using *p*-nitrophenol, a well known substrate for UDP-glucuronyltransferases (UGT). We investigated whether the inhibition was exerted by the glucuronidation of MU using both high pressure liquid chromatography and TLC analyses. The production of MU-glucuronic acid (GlcUA) was consistent with the inhibition of HA synthesis in HAS transfectants. MU-GlcUA was also detected at a similar level in control cells, suggesting that the glucuronidation was mediated by an endogenous UGT. Elevated levels of UGT significantly enhanced the inhibitory effects of MU. In contrast, the inhibition by MU was diminished to the control level when an excess of UDP-GlcUA was added to the cell-free HA synthesis system. We propose a novel mechanism for the MU-mediated inhibition of HA synthesis involving the glucuronidation of MU by endogenous UGT resulting in a depletion of UDP-GlcUA.**

There are a considerable number of reports showing that the biosynthesis of hyaluronan (HA)[1] is elevated in disorders such as fibroses of organs, diseases associated with inflammation, and some types of tumors including mesothelioma and Wilm's tumor (1–5). For instance, accumulation of HA is associated with the progression of atherosclerosis (6). During the progression of hepatitis, HA derived from the Ito cells accumulates in the liver, causing fibrosis and eventually cirrhosis of the liver (7). Because HA is directly associated with liver fibrosis, it has long been utilized as a marker for the diagnosis of chronic hepatitis (8). Also, an exponential increase of HA in the endocervical canal at inappropriate stage of pregnancy can result in miscarriage (9). Recent genetic approaches showed that overproduction of HA accelerated tumor growth and is associated with cancer metastasis (10–14).

HA is a nonsulfated linear glycosaminoglycan composed of thousands of repeating units of GlcNAc-$\beta$(1→4)-GlcUA-$\beta$(1→3) (15). In vertebrates, this molecule is a ubiquitous component of the extracellular matrix and plays critical roles in dynamic functions such as embryonic development, tissue regeneration, and cell migration (16). Both eukaryotic and prokaryotic HA synthases (HAS) catalyze the transglycosylation from both UDP-GlcUA and UDP-GlcNAc donors (17). Following the first cloning of a HAS gene from *Streptococcus* in 1993, three distinct mammalian isoforms, HAS1, HAS2, and HAS3, have been identified and characterized from mouse, human, and other species (17). Considerable progress in understanding HA biosynthesis and its biological functions has been made in recent years.

Identification of a specific inhibitor for HA biosynthesis would not only help elucidate the functions of HA but would also have applications in clinical medicine for the treatment of diseases caused by elevated levels of this glycosaminoglycan. Over the past few decades many researchers have attempted without success to discover specific inhibitors of HA synthesis in mammalian cells (18–22). 4-Methylumbelliferone (MU, 7-hydroxy-4-methyl-2*H*-1-benzopyran-2-one) was found previously to inhibit HA synthesis in cultured human skin fibroblasts but had no effect on the synthesis of any other glycosaminoglycan (23, 24). Since then MU has been used as an

* This work was supported by grants from the CREST of Japan Science and Technology Agency, a preparatory grant for research at the Division of Matrix Glycoconjugates, Research Center for Infectious Disease, Aichi Medical University, grants-in-aid for young scientists (B), Grants-in-aid for Scientific Research on Priority Areas from the Japan's Ministry of Education, Culture, Sports, Science, and Technology 14780480 and 15040203, Grant-in-aid for Scientific Research (B) from Japan Society for the Promotion of Science 15370041, the Aichi Cancer Research Foundation, grant-in-aid from the Tokyo Biochemical Research Foundation, special research funds from Seikagaku Corp., and the Karoji Memorial Fund for Medical Research (A) and (B) in Hirosaki University. The costs of publication of this article were defrayed in part by the payment of page charges. This article must therefore be hereby marked "*advertisement*" in accordance with 18 U.S.C. Section 1734 solely to indicate this fact.

‖‖ To whom correspondence should be addressed. Tel.: 81-52-264-4811 (ext. 2095); Fax: 81-561-63-3532; E-mail: itano@amugw.aichi-med-u.ac.jp.

[1] The abbreviations used are: HA, hyaluronan; MU, 4-methylumbelliferone; *p*NP, *p*-nitrophenol; GlcUA, glucuronic acid; GlcNAc, *N*-acetylglucosamine; Glc, glucose; HA synthase, HAS; $Me_2SO$, dimethyl sulfoxide; PBS, phosphate buffered saline; DTT, dithiothreitol; UGT, UDP-glucuronosyltransferase; HPLC, high pressure liquid chromatography; ELISA, enzyme-linked immunosorbent assay; RT, reverse transcriptase.

inhibitor of HA synthesis in many studies on the functions of HA, although its precise mechanism has not been established in mammalian cells (10, 25, 26).

For many years MU has been used safely in human medicine as a cholagogue by oral administration (27). The clinical application of MU for controlling HA synthesis could potentially prevent malignant alteration of cancer cells and fibrosis of organs. It would therefore be helpful to clarify the inhibition mechanism of MU in mammalian cells. The information may also be useful in developing new compounds that are more effective inhibitors and/or display lower cytotoxicity than MU. A possible phospholipid-dependent inhibition mechanism of MU was found using group C *Streptococcus* in our previous paper (28). We suggested that MU treatment may inhibit HAS activity by altering the distribution of cardiolipin species surrounding HAS in the plasma membrane. However, the change in the distribution of cardiolipin cannot by itself account for the observed inhibition of HA synthesis. Furthermore, the proposed mechanism of inhibition involving cardiolipin might be specific for *Streptococcus*, because mammalian cells have low levels of cardiolipin in the plasma membrane. Indeed the effect of cardiolipin on enzymatic activity is distinct between mammalian HAS1 and streptococcal HAS (29), suggesting that the MU-mediated inhibition is quite complex. In this study we demonstrate a UGT-dependent inhibition mechanism for HA synthesis in mammalian cells using transfectants that express mouse HAS2. We propose the inhibition of HA synthesis is due, in part, to a depletion in the pool of UDP-GlcUA, a common substrate of HAS and UGT.

## EXPERIMENTAL PROCEDURES

*Materials and Reagents*—MU was purchased from Wako Pure Chemicals (Osaka, Japan). *p*-Nitrophenol (*p*NP), *p*NP-sugars (*p*NP-Glc, *p*NP-GlcUA, and *p*NP-GlcNAc), and MU-sugars (MU-Glc, MU-GlcUA, and MU-GlcNAc) were from Sigma. MU and MU-sugars were dissolved in dimethyl sulfoxide ($Me_2SO$); *p*NP and *p*NP-sugars were dissolved in ethanol, and the final concentration of these vehicles in the culture medium and the reaction mixtures for the cell-free HA synthesis were adjusted to 0.1%. UDP-[$^{14}$C]GlcUA (313 mCi/mmol) and [$^{14}$C]*p*NP (70 mCi/mmol) were from ICN Biomedicals, Inc. (Irvine, CA) and American Radiolabeled Chemicals Inc. (St. Louis, MO), respectively. UDP-GlcUA, dithiothreitol (DTT), and ATP were from Nakalai Tesque (Kyoto, Japan). UDP-GlcNAc, bovine liver β-glucuronidase, and glutaraldehyde-stabilized sheep erythrocytes were from Sigma. *Streptomyces* hyaluronidase was obtained from Seikagaku Corp. (Tokyo, Japan). Hyaluronic acid "Chugai" quantitative test kit for the sandwich binding protein assay was purchased from Chugai Pharmaceutical (Tokyo, Japan) (30). Recombinant human UGT1A6 and UGT1A7 proteins were from Calbiochem, and their expression vectors were reported previously (31).

*Cell Culture and Transfection*—Stable transfectants were established by transfection of mouse HAS2 and control vector into rat 3Y1 cells as described previously (32). Cells were routinely cultured in Dulbecco's modified Eagle's medium containing 10% fetal calf serum, 2 mM L-glutamine, and 400 μg/ml G418 at 37 °C. pFLAG-HAS2 and human UGT1A6 expression vector were transiently transfected into COS-1 cells by electroporation as described previously (32). The cells were cultured in Dulbecco's modified Eagle's medium containing 10% fetal calf serum and 2 mM L-glutamine at 37 °C.

*Particle Exclusion Assay*—3Y1-HAS2 cells plated at $1 \times 10^3$ cells in a 35-mm dish were cultured for 2 days and then further cultured for a day with or without 300 μM MU. An aliquot of glutaraldehyde-stabilized sheep erythrocytes ($3 \times 10^8$) in PBS was then added to the culture medium. After 15 min, the culture was observed using an inverted phase-contrast microscope (Olympus IMT-2) (33).

*Quantitative Analyses of the HAS Transcripts*—The relative level of HAS expression in the HAS2 transfectants was determined by real time quantitative RT-PCR as described previously (11). The gene-specific PCR primers and probes were designed from the mouse HAS2 and rat HAS sequences using the Primer Express software (Applied Biosystems, Foster City, CA). The sequences of the various oligonucleotides are as follows: the forward primer for mouse HAS2 was 5′-CCTCGGAATCACAGCTGCTTATA-3′, and the reverse primer was 5′-CTGCCCATAACTTCGCTGAATA-3′; the probe for mouse HAS2 was 5′-TCGCATCTCATCATCCAAAGCCTCTTTG-3′; the forward primer for rat HAS1 was 5′-GGAGATGTGAGAATCCTTAACCCTC-3′, and the reverse primer was 5′-TGCTGGCTCAGCCAACGAAGGAA-3′; the probe for rat HAS1 was 5′-CAGAGCTACTTTCACTGTGTGTCCTGCATC-3′; the forward primer for rat HAS2 was 5′-CCTCGGAATCACAGCTGCTTATA-3′, and the reverse primer was 5′-CTGCCCATGACTTCACTGAAGA-3′; the probe for rat HAS2 was 5′-TCACACCTCATCATCCAAAGCCTCTTTG-3′; the forward primer for rat HAS3 was 5′-GGTACCATCAGAAGTTCCTAGGCAGC-3′, and the reverse primer was 5′-GAGGAGAATGTTCCAGATGCG-3′; and the probe for rat HAS3 was 5′-TGGCTACCGGACTAAGTATACAGCACGCTC-3′. Total RNA was isolated from subconfluent rat 3Y1 cells expressing mouse HAS2 using the RNeasy mini kit (Qiagen, Valencia, CA). Two hundred nanograms of total RNA was used for real time RT-PCR and subsequent analysis. The reaction master mix was prepared to give final concentrations of 1× TaqMan EZ buffer, 0.3 mM dATP, 0.3 mM dCTP, 0.3 mM dGTP, 0.6 mM dUTP, 6 mM manganese acetate, 0.01 units/μl uracil *N*-glycosylase, 0.1 units/μl rTth DNA polymerase, 200 nM primers, and 100 nM TaqMan probe. The conditions for RT-PCR are as follows: 1 cycle at 50 °C for 2 min, 1 cycle at 60 °C for 30 min, 1 cycle at 95 °C for 5 min, 50 cycles at 95 °C for 20 s, and 60 °C for 1 min. Fluorescent signals generated during PCR amplifications were monitored in real time using the 7700 sequence detector system (Applied Biosystems) and analyzed with the sequence detector 1.7 program (Applied Biosystems). The relative amount of glyceraldehyde-3-phosphate dehydrogenase mRNA was measured using the TaqMan rodent glyceraldehyde-3-phosphate dehydrogenase detection reagents (Applied Biosystems). The amount of HAS mRNA was divided by the amount of glyceraldehyde-3-phosphate dehydrogenase mRNA in each sample. The normalized values were designated as the "relative expression coefficient" in this study. Standard curves were generated by serial dilution of total RNA isolated from HAS2 transfectants.

*Determination of the HA Concentration by ELISA-like Assay*—Cells were plated at a density of $1 \times 10^5$ and $8 \times 10^5$ cells/well in a 6-well plate (defined as exponentially growing phase and confluent phase, respectively). The cells were cultured with various concentrations of MU for 24 h. HA released into the culture medium was quantified by an ELISA-like assay using HA-binding protein according to the manufacturer's instructions for the hyaluronic acid "Chugai" quantitative test kit (30). The quantity of HA was expressed per live cell number. The viability of cells was assessed by trypan blue staining.

*HA Synthase Assay*—HAS activity was monitored in the cell-free HA synthesis system using UDP-[$^{14}$C]GlcUA and UDP-GlcNAc as donors and a membrane-rich fraction of the transfectants as an enzyme source as described previously (32). Briefly, the HAS transfectants were washed, harvested, and disrupted by sonication in 10 mM Hepes-NaOH, pH 7.1, 0.5 mM dithiothreitol containing 0.25 M sucrose. Suspensions of the disrupted cells were ultracentrifuged in a Beckman TLS rotor at 43,000 rpm for 1 h to give the high speed pellet. The crude membrane fractions prepared from HAS transfectants were resuspended with standard reaction mixture (0.1 ml of 25 mM Hepes-NaOH, pH 7.1, 5 mM DTT, 15 mM $MgCl_2$, 0.1 mM UDP-GlcNAc, 2 μM UDP-GlcUA, and 0.2 μCi of UDP-[$^{14}$C]GlcUA) and incubated at 37 °C for 1 h. Depending on the type of experiment, MU, *p*NP, and their sugar derivatives were added to the reaction mixture. Alternatively, the membrane fractions were preincubated at 37 °C for 1 h with 300 μM MU or 300 μM MU-GlcUA in the preincubation mixture (0.1 ml of 25 mM Hepes-NaOH, pH 7.1, 5 mM DTT, 15 mM $MgCl_2$, 0.1 mM UDP-GlcUA), and then HA synthesis was initiated by adding 2 mM UDP-GlcNAc and 0.2 μCi of UDP-[$^{14}$C]GlcUA. The reaction was terminated at the indicated time by addition of SDS to 2% (w/v). The mixtures were then spotted onto Whatman No. 3MM paper, and the paper was developed in 1 M ammonium acetate (pH 5.5) and ethanol (65:35 v/v) for 3 days. The origin, containing the synthesized polymers, was removed, and the amount of radioactivity in the high molecular mass HA was determined by liquid scintillation counting.

*Agarose Gel Electrophoresis of HA*—The size distribution of radiolabeled HA synthesized in the cell-free reaction was analyzed by agarose gel electrophoresis (0.5% gel) as described previously (32). The synthesized HA was incubated at 37 °C for 1 h with or without 1 turbidity reducing unit of *Streptomyces* hyaluronidase prior to loading on the gel. After drying the gel, the radioactive HA was detected using a BAS 5000 Bio-Imaging Analyzer (Fuji Film Co., Tokyo, Japan).

*HPLC Analysis of the MU-sugar Derivative*—MU-sugar derivatives, from culture conditioned medium and from cell lysate, were analyzed by HPLC using a TSK gel ODS-120T (15 cm × 4.6 mm inner diameter) column. HPLC conditions were identical to those described by

Zimmerman *et al.* (34). Eluted fractions were monitored by detecting fluorescence (excitation 325 nm, emission 380 nm) using a fluorescence spectrophotometer Hitachi F-1050 (Tokyo, Japan). Cells were washed with PBS three times and then disrupted in a solution of 2% SDS-PBS by sonication for 2 min (4 bursts of 30 s) using a sonifier (model UR-20P, Tomy Seiko, Tokyo, Japan). The cell lysate was then obtained by centrifugation at 105,000 × *g* for 30 min. The supernatants were used for HPLC analysis. For TLC analysis in Fig. 3 and for mass spectrometry, a peak corresponding to MU-GlcUA was collected by HPLC as described below. A fraction containing MU-GlcUA was prefractionated from culture supernatant using a Sep-Pac Plus C18 cartridge (Waters, MA) prior to HPLC. Briefly, the culture supernatant was loaded onto the cartridge, and the cartridge was then washed with water. Bound materials containing MU-GlcUA were eluted with 100% methanol, concentrated by using a vacuum evaporator centrifuge (Iwaki, Tokyo, Japan), and analyzed by HPLC. A peak of MU-GlcUA was collected and desalted using a Sep-Pac Plus C18 cartridge. After drying, the residue was dissolved into methanol and analyzed by TLC or mass spectrometry.

*TLC Analysis of the MU-sugar or pNP-sugar Derivative*—Radiolabeled MU-sugar or *p*NP-sugar derivatives produced in the cell-free HA synthesis system was treated with or without 2 units of β-glucuronidase at 37 °C for 1 h and then separated by TLC. TLC was performed on a Silica 60 TLC plate (Merck) using 1-butanol/ethanol/water (5:3:2, v/v/v) as the mobile phase (35). After drying the plate, radioactive spots were detected using a BAS 5000 Bio-Imaging Analyzer. The radiolabeled product derived from the incubation of *p*NP and UDP-[$^{14}$C]GlcUA according to the standard assay method of UGT (36) was used for determining the mobility of *p*NP-GlcUA. Fluorescent spots containing MU or MU-sugar were detected by ultraviolet irradiation using a transilluminator. Authentic MU-GlcUA was used as a standard.

*Mass Spectrum Measurements*—Mass spectra were obtained on a PE-Sciex API-100 single-quadrupole mass spectrometer (Thornhill, Ontario, Canada) equipped with an atmospheric pressure ionization source described previously (37). The mass spectrometer was operated in the negative mode. Samples dissolved in 50% 2-propanol were ionized by electrospray ionization and continuously infused into the electrospray ionization chamber at a flow rate of 5 μl min$^{-1}$.

## RESULTS

*Inhibitory Effect of MU on HA Production and HA Matrix Formation of the HAS2-expressing Cells*—MU was originally found to inhibit HA synthesis and HA matrix formation of cultured human skin fibroblasts (23, 24). The recent discovery that MU inhibits HA synthesis of group C *Streptococcus* in a phospholipid-dependent fashion provided new insight into understanding the mechanism of inhibition (28). However, the inhibition of HA synthesis by MU cannot be explained by this mechanism alone, particularly in mammalian cells. In this study, we examined the effects of MU on HA synthesis by using HAS2 overexpressing cells in order to clarify which step of HA synthesis is the target for the inhibition. The HAS2 overexpressing cells, named 3Y1-HAS2, were established from rat 3Y1 fibroblasts by transfection with HAS2 cDNA as described previously (32). Formation of pericellular HA matrices and HA production were significantly inhibited in 3Y1-HAS2 cells by treatment with MU as observed previously in cultured human skin fibroblasts (23, 24) (Fig. 1). The formation of pericellular HA matrices was inhibited by ~30% during exposure to 300 μM MU compared with the nontreated control. The level of inhibition was even more apparent at higher concentrations of MU (data not shown). HA accumulation in the conditioned medium was dose-dependently decreased by MU treatment both in the exponentially growing and confluent phases of 3Y1-HAS2 cells (Fig. 1*E*).

Transcription of the mouse HAS2 transgene and the endogenous HAS genes in the transfectants was assessed by real time RT-PCR using mouse- and rat-specific HAS primers and probes. No obvious change in the transcriptional levels of these HAS genes was observed at the low or moderate concentrations of MU, whereas the level of the endogenous HAS2 gene was inhibited during exposure to a high dose of MU (Table I). These results suggest that MU inhibits HAS activity post-transcriptionally at the low or moderate concentrations of MU. In contrast, a high dose of MU inhibits HA synthesis by suppressing HAS functions both transcriptionally and post-transcriptionally.

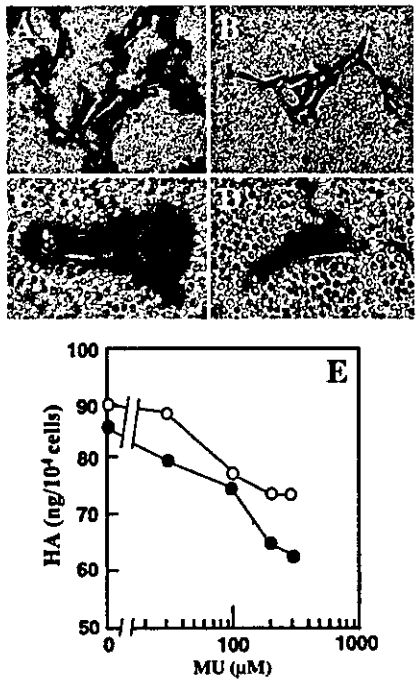


FIG. 1. **HA production and matrix formation of HAS2 transfectants after MU treatment.** *A–D*, pericellular HA matrices surrounding 3Y1-HAS2 transfectants were visualized by the particle exclusion assay, and photomicrographs were taken under inverted phase contrast microscope at ×300 (*A* and *B*) and then magnified further (*C* and *D*). The 3Y1-HAS2 cells were cultured for 24 h with (*B* and *D*) or without (*A* and *C*) 300 μM MU. *E*, the HA contents in the conditioned medium from exponentially growing (*open circles*) and confluent cultures (*closed circles*) were measured by ELISA-like assay at 24 h after the treatment of 3Y1-HAS2 transfectants with various concentrations of MU. Data represent average of two independent experiments.

TABLE I
*Relative HAS expression in HAS2 transfectants after MU treatment*

| MU | Mouse HAS2 | Rat HAS2 | Rat HAS3 |
|---|---|---|---|
| μM | % | % | % |
| 0 | 100 | 100 | 100 |
| 10 | 130.7 ± 19.7 | 94.7 ± 25 | 98.5 ± 13.9 |
| 30 | 129.1 ± 34.8 | 86.1 ± 10.7 | 93.1 ± 13.7 |
| 100 | 137.4 ± 11.6 | 105.0 ± 28 | 93.9 ± 10.3 |
| 300 | 93.3 ± 29.6 | 77.1 ± 4.3 | 90.4 ± 2.1 |
| 1000 | 104.8 ± 28.4 | 48.6 ± 8.2 | 97.4 ± 10.6 |

*Effect of MU on HA Synthesis and Chain Elongation in a Cell-free HA Synthesis System*—Cell-free HA synthesis was examined by using the membrane-rich fraction of 3Y1-HAS2 cells. As shown in Fig. 2*A*, HAS activity was inhibited by MU in a dose-dependent manner, and the inhibition reached to 50% of the nontreated control at 300 μM MU. The inhibitory effect was observed at an early stage of HA synthesis and reached a plateau 30 min after treatment with MU (Fig. 2*B*). The size distribution of HA synthesized in the cell-free system was also determined by agarose gel electrophoresis (Fig. 2, *C* and *D*). The decrease in the molecular size of HA was caused by MU treatment in both a dose- and time-dependent manner. These data suggest MU inhibits HA synthesis by suppressing HAS function post-transcriptionally. Furthermore, the MU-mediated inhibition of HA synthesis may be caused by direct inhibition of HAS activity.

MU has been used as a substrate to measure the activity of UGTs, which are involved in the detoxification of phenolic